Biology | Faculty Publications & Research

2017

Northern Spotted Owl (Strix occidentalis caurina) Genome: Divergence with the Barred Owl (Strix varia) and Characterization of Light-Associated Genes

Christopher A. Emerling
cemerlin@whittier.edu

Zachary R. Hanna

James B. Henderson

Jeffrey D. Wall

Jérôme Fuchs

See next page for additional authors

Recommended Citation

Hanna, Z. R., Henderson, J. B., Wall, J. D., Emerling, C. A., Fuchs, J., Runckel, C., ... & Dumbacher, J. P. (2017). Northern spotted owl (Strix occidentalis caurina) genome: divergence with the barred owl (Strix varia) and characterization of light-associated genes. Genome biology and evolution, 9(10), 2522-2545.

Authors

Christopher A. Emerling, Zachary R. Hanna, James B. Henderson, Jeffrey D. Wall, Jérôme Fuchs, Charles Runckel, David P. Mindell, Rauri C. K. Bowie, Joseph L. DeRisi, and John P. Dumbacher

Northern Spotted Owl (*Strix occidentalis caurina*) Genome: Divergence with the Barred Owl (*Strix varia*) and Characterization of Light-Associated Genes

Zachary R. Hanna[1,2,3,4,*], James B. Henderson[3,4], Jeffrey D. Wall[1,3,4,5], Christopher A. Emerling[1,2], Jérôme Fuchs[3,6], Charles Runckel[7,8,9], David P. Mindell[1], Rauri C. K. Bowie[1,2], Joseph L. DeRisi[7,8], and John P. Dumbacher[3,4]

[1]Museum of Vertebrate Zoology, University of California, Berkeley, California, USA

[2]Department of Integrative Biology, University of California, Berkeley, California, USA

[3]Department of Ornithology & Mammalogy, California Academy of Sciences, San Francisco, California, USA

[4]Center for Comparative Genomics, California Academy of Sciences, San Francisco, California, USA

[5]Institute for Human Genetics, University of California, San Francisco, California, USA

[6]UMR 7205 Institut de Systématique, Evolution, Biodiversité, CNRS, MNHN, UPMC, EPHE, Sorbonne Universités, Muséum National d'Histoire Naturelle, Paris, France

[7]Department of Biochemistry and Biophysics, University of California, San Francisco, California, USA

[8]Howard Hughes Medical Institute, Bethesda, Maryland, USA

[9]Runckel & Associates, Portland, Oregon, USA

*Corresponding author: E-mail: zachanna@berkeley.edu.

Data deposition: This Whole Genome Shotgun sequencing project has been deposited at DDBJ/ENA/GenBank under the accession NIFN00000000. The version described in this article is version NIFN01000000. Specimen Sequoia blood sample deposited as CAS:ORN:98821, California Academy of Sciences, San Francisco, California, United States. *Strix occidentalis caurina* raw genomic DNA sequences obtained from CAS:ORN:98821 are available from NCBI Sequence Read Archive (SRA) (SRA run accessions SRR4011595, SRR4011596, SRR4011597, SRR4011614, SRR4011615, SRR4011616, SRR4011617, SRR4011618, SRR4011619, and SRR4011620). *Strix varia* raw genomic DNA sequences obtained from CNHM<USA-OH>:ORNITH:B41533 are available from NCBI SRA (SRA run accessions SRR5428115, SRR5428116, and SRR5428117). Program ScaffSplitN50s deposited at Zenodo http://doi.org/10.5281/zenodo.163683 and available from https://github.com/calacademy-research/ScaffSplitN50s. Program dupchk deposited at Zenodo http://doi.org/10.5281/zenodo.163722 and available from https://github.com/calacademy-research/dupchk. Program GItaxidIsVert deposited at Zenodo http://doi.org/10.5281/zenodo.163737 and available from https://github.com/calacademy-research/GItaxidIsVert. Program scafSeqContigInfo deposited at Zenodo http://doi.org/10.5281/zenodo.163748 and available from https://github.com/calacademy-research/scafSeqContigInfo. Program scafN50 deposited at Zenodo http://doi.org/10.5281/zenodo.163739 and available from https://github.com/calacademy-research/scafN50. Additional scripts deposited as NSO-genome-scripts at Zenodo http://doi.org/10.5281/zenodo.805012 and available from https://github.com/calacademy-research/NSO-genome-scripts. Gene and repeat annotation files, the raw variant call file, alignments of light-associated gene orthologs as well as assemblies of transcriptome sequences deposited at Zenodo http://doi.org/10.5281/zenodo.822859.

Abstract

We report here the assembly of a northern spotted owl (*Strix occidentalis caurina*) genome. We generated Illumina paired-end sequence data at $90\times$ coverage using nine libraries with insert lengths ranging from ~250 to 9,600 nt and read lengths from 100 to 375 nt. The genome assembly is comprised of 8,108 scaffolds totaling 1.26×10^9 nt in length with an N50 length of 3.98×10^6 nt. We calculated the genome-wide fixation index (F_{ST}) of *S. o. caurina* with the closely related barred owl (*Strix varia*) as 0.819. We examined 19 genes that encode proteins with light-dependent functions in our genome assembly as well as in that of the barn owl (*Tyto alba*). We present genomic evidence for loss of three of these in *S. o. caurina* and four in *T. alba*. We suggest that most light-

associated gene functions have been maintained in owls and their loss has not proceeded to the same extent as in other dim-light-adapted vertebrates.

Key words: nuclear genome, bird, Strigidae, Strigiformes, Aves.

Introduction

The spotted owl (*Strix occidentalis*) is a large, charismatic inhabitant of dense forests whose range extends along the Pacific coast of North America from southwestern British Columbia to southern California and eastward into the southwest desert states and Mexico. The northern spotted owl subspecies, *S. o. caurina*, inhabits the Pacific Northwest portion of the *S. occidentalis* range from British Columbia south along the west coast to the Golden Gate strait, California. The US Fish and Wildlife Service listed *S. o. caurina* as "threatened" under the Endangered Species Act (ESA) in 1990 (Thomas et al. 1990) and the owl has been the subject of much ecological research and economic tension. Since its listing under the ESA, populations have continued to decline (Forsman et al. 1996, 2011; Dugger et al. 2015; Davis et al. 2016) despite the increased level of protection. Although it is not considered a "model species" by most researchers, there is a considerable amount of demographic and ecological data available for this species (Courtney et al. 2004), especially in comparison with other owls, which tend to be less studied than diurnal birds.

Spotted owl conservation efforts often focus on genetic challenges, including those relating to small population sizes and inbreeding, relationships to other population segments, and potential interbreeding with congeners (Barrowclough et al. 1999, 2005, 2011; Haig et al. 2001, 2004). A complete genome assembly could provide many useful tools for conservation geneticists, including independent estimates of effective population size (N_e), tools for identifying and developing genetic markers such as single nucleotide polymorphisms and microsatellites, and data that can provide direct and relatively accurate measures of interbreeding.

The congeneric barred owl (*Strix varia*), formerly native to North America east of the Rocky Mountains (Mazur and James 2000), has invaded western North America in the last 50–75 years and, from British Columbia to southern California, has become broadly sympatric with the spotted owl in the last 50 years (Taylor and Forsman 1976; Livezey 2009a, 2009b) and likely poses a threat to the survival of the northern spotted owl (Forsman et al. 2011; Wiens et al. 2014; Dugger et al. 2015; Diller et al. 2016). In addition to competing for western forest habitat, barred and spotted owls interact at the genetic level as they can hybridize and successfully backcross (Haig et al. 2004; Kelly and Forsman 2004; Funk et al. 2007). Much of our motivation to assemble the northern spotted owl genome was to provide a resource to aid those studying the genetics of this owl and related taxa.

Thus, we included analyses of the genome of a barred owl from eastern North America as a baseline comparison to the spotted owl. We compared genome-derived estimates of N_e from both species and calculated F_{ST} between them.

Access to high-coverage, relatively complete genomes also allows researchers to address questions that, without this resource, are inaccessible or difficult to answer. For example, previous work has suggested that owls have evolved an atypical avian visual system with high numbers of dim-light-adaptive rod photoreceptors (Fite 1973; Bowmaker and Martin 1978) and a diminished capacity for color vision (Bowmaker and Martin 1978; Wu et al. 2016). Whole genome sequencing can establish what mutation(s) or genomic rearrangements resulted in their reduced color vision and, with multiple genomes, one may test whether such mutations are lineage-specific or inherited from a common ancestor. The genome assembly of the barn owl (*Tyto alba*; Aves: Tytonidae) was available and allowed us to test owl-lineage-based hypotheses, but it was one of the lower-coverage, less complete of the available avian genome assemblies (Zhang, Li B, Li C, et al. 2014). A complete spotted owl genome, in addition to providing whole genome data for a representative of Strigidae, the other of the two families of owls, could also enable a definitive search for genes involved in nocturnal visual adaptations and a better understanding of the processes of mutation that lead to such adaptations.

Materials and Methods

Genome Sample

We collected blood from a captive adult northern spotted owl (*S. o. caurina*) at WildCare rehabilitation facility in San Rafael, California. The captive owl, named Sequoia and referred to as such hereafter, patient card No. 849, was admitted to WildCare on 5 June 2005 as an abandoned nestling found in Larkspur, Marin County, California (CAS:ORN:98821; table 1). We chose to sequence the genome of this individual as *S. occidentalis* is known to hybridize with *S. varia* (Haig et al. 2004; Kelly and Forsman 2004; Funk et al. 2007) and we wanted to ensure that we were sequencing the genome of a nonhybrid, nonintrogressed individual. The first Marin County *S. varia* detections occurred in 2003 and researchers estimated a population size of only three individuals by 2005 (Jennings et al. 2011). First generation hybrid individuals are phenotypically diagnosable with intermediate plumage characteristics (Hamer et al. 1994). Thus, if Sequoia had any *S. varia* genetic material, it would likely have been a first

Table 1

Specimen Data

Specimen	County	State	Country	Date	Specimen Institution
CAS:ORN:98821	Marin County	CA	United States	26 Jun 2005	California Academy of Sciences
CNHM<USA-OH>:ORNITH	Hamilton County	OH	United States	29 Nov 2010	Cincinnati Museum Center

Note.—Information regarding the *S. o. caurina* and *S. varia* individuals from which we obtained genomic sequences for this study including the county, state, country, and date of collection for each specimen as well as the specimen code and institution where each specimen is archived.

generation hybrid and easily diagnosable as such. No plumage or behavioral features, such as vocalizations, suggested that it was a hybrid individual.

DNA Isolation

For genomic DNA libraries that required very high molecular weight DNA, we isolated DNA by using the precipitation method provided by the Gentra Puregene Kit (Qiagen, Netherlands) and following the manufacturer's protocol. We also isolated DNA using a column-based method, the DNeasy Blood & Tissue Kit (Qiagen, Netherlands), and used this DNA for those libraries where very high molecular weight was not essential. We assessed the quality and concentration of all isolated DNA using a Nanodrop 2000c spectrophotometer (Thermo Fisher Scientific, USA), 2100 BioAnalyzer (Agilent Technologies, USA), Qubit 2.0 Flurometer (Invitrogen, USA), and by running the DNA on a 1% agarose gel. We determined that the resulting DNA from both methods had high molecular weight with most of the DNA comprising fragments >50,000 nucleotides (nt) in length.

Illumina Data

We obtained paired-end Illumina data from nine whole-genome libraries constructed using a variety of methods with a range of average insert lengths from 247 to 9,615 nt. In our library construction we utilized a range of DNA shearing methods including enzyme-based, ultrasonication, and hydro-dynamic forces using a Hydroshear DNA Shearing Device (GeneMachines, USA). We amplified all but one of the libraries using polymerase chain reaction (PCR) and sequenced them with read lengths from 100 to 375 nt (see supplementary table S1, Supplementary Material online; supplementary section 1.1–1.8, Supplementary Material online).

Trimming, Merging, Error-Correction

We trimmed the Nextera mate-pair data using the software NxTrim version 0.2.3-alpha (O'Connell 2014; O'Connell et al. 2015) (supplementary section 1.9.1, Supplementary Material online) in order to classify reads of mate pair libraries as true mate pair reads, paired-end reads, or singleton reads. We then removed adapters and low quality bases separately for the resulting mate-pair sequences, paired-end sequences, and singleton sequences using Trimmomatic version 0.32 (Bolger

et al. 2014) (supplementary section 1.9.2, Supplementary Material online). We also used Trimmomatic to remove adapters from all non-mate-pair libraries (supplementary section 1.10.1, Supplementary Material online). In order to test how various trimming methods affected the assembly outcome, we trimmed to different thresholds for some of our preliminary assemblies by changing the Trimmomatic version 0.32 (Bolger et al. 2014) average quality score parameters. We did not apply the error-correction process to reads trimmed to a stringent quality threshold. For some preliminary assemblies, we performed adapter and quality trimming, but did not merge overlapping paired-end reads (supplementary section 1.13, Supplementary Material online). However, since substantial portions of the paired-end reads from all of the libraries, except the Nextera700 bp library, were overlapping, for the sequences that we used to generate our final assembly we joined overlapping paired reads using BBMap version 34.00 (Bushnell 2014) (supplementary section 1.10.2, Supplementary Material online). We then performed quality trimming on the non-mate-pair library data using Trimmomatic version 0.32 (Bolger et al. 2014) (supplementary section 1.10.3, Supplementary Material online). Since we trimmed using the relatively lenient threshold of trimming the read when the average quality over 4 bp dropped below quality score (Phred) 17, we next used the k-mer-based error corrector in the SOAPdenovo2 toolkit, SOAPec version 2.01 (Luo et al. 2012), to correct sequence errors (supplementary section 1.11, Supplementary Material online). For any read that became unpaired due to the loss of the paired read we separately subjected it to the same adapter, quality trimming, and error-correcting steps as the reads that remained paired (supplementary section 1.12, Supplementary Material online).

Genome Size

In order to estimate the *S. occidentalis* nuclear genome size from our Illumina data, we ran Preqc (Simpson 2014) with the paired-end sequences from the Nextera700 bp data set (supplementary section 1.14, Supplementary Material online).

Assembly

We assembled the *S. occidentalis* genome using SOAPdenovo2 version 2.04 (Luo et al. 2012). In order to determine the optimal assembly parameter options, we performed numerous trial runs experimenting with different k-

mer values and parameters. We utilized the insert size estimated in the output of trial assemblies to refine our estimation of the insert sizes for our libraries and used these refined values as input into subsequent assembly configuration files (supplementary table S1, Supplementary Material online). After optimizing the SOAPdenovo2 assembly options, we generated fourteen further preliminary assemblies to test how using differently filtered versions and subsets of our Illumina sequence data affected the assembly outcome. We examined how the assembly was affected by trimming our data to multiple quality thresholds, using or not applying error correction, not merging or merging our overlapping paired-end data, assembling with different k-mers, using or not using singleton data, and dropping certain libraries (supplementary table S2, Supplementary Material online). We used dupchk (Henderson and Hanna 2016a) to check for sequence duplication in each sequenced library and found an elevated level of duplication in the Hydroshear library data, so we excluded all sequences from this library from several assemblies (supplementary section 1.15, Supplementary Material online).

Preliminary Assembly Assessment

In order to compare our preliminary assemblies, we removed contiguous sequences (contigs) or scaffolds less than or equal to 300 nt with the intent of removing any unassembled reads from the assembly. We calculated the contig and scaffold N50 as well as the number of scaffolds in various length classes using scafN50 (Henderson and Hanna 2016d). We calculated the total length of the assembly, the percentage of "N" characters in the assembly that represent sequence gaps between contiguous sequences joined by paired-end or mate-pair data (% N's), and the total number of scaffolds using scafSeqContigInfo (Henderson and Hanna 2016e). We were conservative in the calculation of these metrics and separated scaffolds into contigs at each N in the sequence. We then used CEGMA version 2.5 (Parra et al. 2007) to annotate a set of highly conserved eukaryotic genes (CEGs) in our assembly and thereby obtain an assessment of the quality and completeness of each assembly (supplementary section 1.16, Supplementary Material online).

We found it useful to assess the genome assembly's continuity and completeness at each stage of the assembly process. We searched for CEGs using CEGMA to evaluate our earlier assemblies. However, at this time, one of the CEGMA tool authors recommends that researchers use BUSCO in place of CEGMA (Bradnam 2015). Since we used CEGMA to evaluate our earliest assemblies, we continued to use CEGMA for continuity. We ran BUSCO on our final assembly and the results suggested similar completeness as those of CEGMA.

Determination of Final Assembly

We examined multiple statistics in choosing our final assembly. We valued high contig and scaffold N50 values, low % N's in the sequence, a low total number of scaffolds, larger numbers of scaffolds longer than 1 mega nucleotide (Mnt), and completeness as reflected in the number of conserved genes found by the CEGMA pipeline. We decided that the assembly that had the best statistics across these categories was assembly 4 (table 2) and proceeded forward with this assembly.

We filled gaps in the assembly using the gap closing tool in the SOAPdenovo2 toolkit, GapCloser version 1.12-r6 (Luo et al. 2012). The gap-closed assembly contained many sequences under 1,000 nt in length, a substantial portion of which appeared to be unassembled reads. We used ScaffSplitN50s (Henderson and Hanna 2016c) to compare statistics describing the continuity of the assembly after removing contigs/scaffolds of lengths 300, 500, and 1,000 nt as well as when using N blocks of lengths 1, 5, 10, 15, 20, and 25 to separate contigs within scaffolds. We decided to remove all contigs and scaffolds <1,000 nt for downstream analyses and will refer to the resulting assembly as "StrOccCau_0.2" hereafter (supplementary section 1.18, Supplementary Material online).

Final Assembly Statistics

We calculated basic statistics on StrOccCau_0.2 using the "assemblathon_stats.pl" script, which was used for comparison of the Assemblathon 2 genome assemblies (Bradnam et al. 2013). We used both CEGMA version 2.5 (Parra et al. 2007) and BUSCO version 1.1b1 (Simão et al. 2015a, 2015b) to annotate sets of CEGs and thereby assess the assembly's completeness (supplementary section 1.19, Supplementary Material online). We also calculated basic statistics and ran CEGMA as described earlier for other available avian genomes, including the barn owl (*T. alba*) (Zhang, Li, Gilbert, et al. 2014a; Zhang, Li C, et al. 2014), downy woodpecker (*Picoides pubescens*) (Zhang, Li, Gilbert, et al. 2014b; Zhang, Li C, et al. 2014), zebra finch (*Taeniopygia guttata*) (GenBank assembly accession GCA_000151805.2; Warren et al. 2010), bald eagle (*Haliaeetus leucocephalus*) (Warren et al. 2014; Zhang, Li C, et al. 2014), golden eagle (*Aquila chrysaetos*) (GenBank assembly accession GCA_000766835.1; Wesley Warren et al. 2014), chimney swift (*Chaetura pelagica*) (Zhang, Li, Gilbert, et al. 2014c; Zhang, Li C, et al. 2014), and chicken (*Gallus gallus*) (GenBank assembly accession GCA_000002315.3; Warren et al. 2017).

Contamination Assessment

To assess whether any assembled contigs were derived from contaminant nonvertebrate organisms, we performed a local alignment of all sequences in StrOccCau_0.2 to a copy of the

Table 2

Metrics of Preliminary Assemblies

Assembly	contig N50 (nt)	scaffold N50 (nt)	Total Length of Assembly (Gnt)	Ns (%)	Total Number of Scaffolds	Number Of Scaffolds > 1 Mnt In Length	Partial CEGs Found by CEGMA	Complete CEGs Found by CEGMA
1	9,499	3,869,235	1.275	4.77	51,843	292	231	205
2	12,096	3,522,724	1.274	4.40	48,264	295	233	205
3	10,425	4,007,375	1.272	4.88	47,075	0	226	200
4*	**13,983**	**3,919,460**	**1.275**	**4.26**	**47,900**	**303**	**235**	**221**
5	10,315	4,164,870	1.272	4.45	46,146	287	232	206
6	9,142	3,780,867	1.275	4.86	51,615	296	230	202
7	9,802	3,478,271	1.274	4.42	54,240	327	233	209
8	12,650	3,665,028	1.271	4.18	43,092	313	231	204
9	12,006	3,587,241	1.271	4.66	44,939	307	226	201
10	12,487	3,586,666	1.271	4.26	44,345	314	232	204
11	14,651	3,917,141	1.276	4.26	50,636	293	234	217
12	14,627	3,728,521	1.276	4.28	50,349	305	234	219
13	14,672	3,917,121	1.276	4.26	50,129	293	234	217
14	13,967	3,431,044	1.300	4.50	127,384	318	238	218

NOTE.—Various continuity and completeness summary statistics for our preliminary assemblies. We removed contigs/scaffolds <300 nt in order to remove unassembled reads from the assemblies before calculating these statistics. We defined contigs with the very restrictive parameter that each N split a scaffold into a separate contig. "Partial CEGs found by CEGMA" refers to the number of gene sequences found by CEGMA in the assembly in at least partial completeness out of 248 total CEGs. An asterisk and bolded font mark the preliminary assembly that we chose to use as the basis for the final assembly.

NCBI nucleotide database "nt" (Clark et al. 2016; NCBI Resource Coordinators 2016) using NCBI's BLAST+ version 2.3.0 tool BLASTN (Altschul et al. 1997; Camacho et al. 2009). We searched for nonvertebrate hits in the top aligned sequences using a local copy of the NCBI taxonomy database (ftp://ftp.ncbi.nlm.nih.gov/pub/taxonomy; Clark et al. 2016; NCBI Resource Coordinators 2016) and GItaxIdIsVert (Henderson and Hanna 2016b). We re-examined those sequences where any of the five output alignments was an alignment to a nonvertebrate using the web version of NCBI's BLAST+ version 2.4.0 tool BLASTN (Altschul et al. 1997; Camacho et al. 2009). We used bioawk version 1.0 (Li 2013b) to remove contaminant scaffolds from the assembly and will refer to the resulting assembly version hereafter as "StrOccCau_1.0." We calculated basic statistics on StrOccCau_1.0 using the "assemblathon_stats.pl" script (Bradnam et al. 2013) (supplementary section 1.20, Supplementary Material online). We confirmed that no CEGs were present in the contaminant scaffolds.

Mitochondrial Genome Identification

We searched for any contigs or scaffolds that were assemblies of the mitochondrial genome, rather than the nuclear genome by aligning a mitochondrial genome assembly of the brown wood owl (*Strix leptogrammica*) (GenBank Accession KC953095.1; Liu et al. 2014) to StrOccCau_1.0 using NCBI's BLAST+ version 2.4.0 tool BLASTN (Altschul et al. 1997; Camacho et al. 2009). We searched for long alignments to scaffolds with lengths not greatly exceeding 16,500 nt, the approximate size of the mitochondrial genomes of other owl

(Aves: Strigiformes) species (Harrison et al. 2004; Liu et al. 2014; Mahmood et al. 2014; Hengjiu et al. 2016). We extracted the scaffold corresponding to the mitochondrial genome assembly using bioawk version 1.0 (Li 2013b) and annotated it using the MITOS WebServer version 806 (Bernt et al. 2013) (supplementary section 1.21, Supplementary Material online). We will refer to the mitochondrial and nuclear genome assemblies hereafter as StrOccCau_1.0_mito and StrOccCau_1.0_nuc, respectively.

Sex Identification

In order to determine the sex of the *S. o. caurina* individual that supplied the genetic sample for this genome assembly, we aligned nucleotide sequences of *S. varia* chromo-helicase-DNA binding protein-W (*CHD1W*) (GenBank Accession KF425687.1) and chromo-helicase-DNA binding protein-Z (*CHD1Z*) (GenBank Accession KF412792.1) to StrOccCau_1.0 using NCBI's BLAST+ version 2.4.0 tool BLASTN (Altschul et al. 1997; Camacho et al. 2009). We extracted the scaffolds that aligned to the *CHD1W* and *CHD1Z* sequences using bioawk version 1.0 (Li 2013b) and then used Geneious version 9.1.4 (Kearse et al. 2012; Biomatters 2016a) to predict the length of a PCR product resulting from amplification of this region with primers 2550 F and 2718 R (Fridolfsson and Ellegren 1999) (supplementary section 1.22, Supplementary Material online).

Repeat Annotation

We ran our genome through two separate series of repeat masking steps. The purpose of the first series was to produce

a masked genome without masking of low complexity regions or simple repeats, which we could then use for downstream annotation steps. The purpose of the second series was to obtain an accurate assessment of the total repeat content of the genome, including low complexity regions and simple repeats. We first performed a homology-based repeat annotation of the genome assembly using RepeatMasker version 4.0.5 (Smit et al. 2013) and the repeat databases of the DFAM library version 1.3 (Wheeler et al. 2013) and the Repbase-derived RepeatMasker libraries version 20140131 (Jurka 1998, 2000; Jurka et al. 2005; Bao et al. 2015) without masking low complexity regions or simple repeats. We next performed a *de novo* modeling of the repeat elements in the genome using RepeatModeler version 1.0.8 (Smit and Hubley 2015) in order to create a database of repetitive regions in our genome assembly. We then further masked the genome by running RepeatMasker using the homology-based repeat-masked genome as input and the repeat database created by our RepeatModeler run and again not masking low complexity regions or simple repeats. The output was a twice-masked genome, hereafter "StrOccCau_1.0_masked." Finally, we repeated the above steps to perform a separate homology-based and *de novo* masking of the genome with RepeatMasker runs that included masking of low complexity regions and simple repeats in order to obtain an accurate estimate of the total repeat content of the genome (supplementary section 1.23, Supplementary Material online).

Gene Annotation

In order to annotate genes in the repeat-masked assembly, StrOccCau_1.0_masked, we followed the MAKER version 2.31.8 (Cantarel et al. 2008) pipeline as described in Campbell et al. (2014). As input for protein homology evidence, we provided MAKER the redundant protein set previously used to annotate 48 avian genomes (Zhang, Li C, et al. 2014). We used the genes found in our CEGMA run to train the gene prediction tool, Semi-HMM-based Nucleic Acid Parser or SNAP version 2006-07-28 (Korf 2004). As we independently performed repeat masking, we ran MAKER without further repeat masking. We combined all of the output gene annotations using the MAKER accessory scripts "fasta_merge" and "gff3_merge" (supplementary section 1.24, Supplementary Material online).

We assigned putative gene functions to the MAKER annotations by comparing the output MAKER protein fasta file to the Swiss-Prot UniProt release 2016_04 (Consortium 2015) database using NCBI's BLAST 2.2.31+ tool "blastp" (Altschul et al. 1997; Camacho et al. 2009). In order to identify proteins with known functional domains, we ran InterProScan version 5.18-57.0 (Jones et al. 2014) on the protein sequences generated by MAKER. We then filtered transcripts with an Annotation Edit Distance (AED) < 1 and/or a match to a domain in Pfam, a database of protein families (Finn et al. 2016), using the script "quality_filter.pl" supplied in MAKER version 3.00.0 (Cantarel et al. 2008). We compared the unfiltered and filtered GFF3 files by analyzing the AED values for all annotations using the script "AED_cdf_generator.pl" supplied in MAKER version 3.00.0 (Cantarel et al. 2008) and graphed the distribution of values using Matplotlib pyplot (Hunter 2007) (supplementary fig. S1, Supplementary Material online). Finally, we used GenomeTools version 1.5.1 (Gremme et al. 2013) to calculate annotation summary statistics, including distributions of gene lengths, exon lengths, number of exons per gene, coding DNA sequence (CDS) lengths (measured in amino acids), and intron lengths (supplementary section 1.24, Supplementary Material online) and graphed these using Matplotlib pyplot (Hunter 2007) (supplementary figs. S2–S6, Supplementary Material online).

Alignment

We aligned the filtered versions of all sequences from all libraries to StrOccCau_1.0_masked using the Burrows-Wheeler aligner, BWA-MEM version 0.7.12-r1044 (Li 2013a), and then merged, sorted, and marked duplicate reads using Picard version 1.104 (http://broadinstitute.github.io/picard; last accessed October 1, 2016). We then assessed the genome coverage, duplication level, and other statistics of each aligned sequence library using Picard version 1.141 (http://broadinstitute.github.io/picard; last accessed October 1, 2016) (supplementary section 1.25, Supplementary Material online). In order to obtain an estimate of the insert size of the mate pair libraries independent of the N-gaps in the scaffold sequences, we divided scaffolds into contigs at 25 or more N's, aligned the mate pair libraries to this set of contigs using BWA-MEM version 0.7.12-r1044 (Li 2013a), and then calculated insert sizes from these alignments (supplementary section 1.25, Supplementary Material online).

Microsatellite Analysis

We searched the repeat-masked and unmasked versions of our assembly for all microsatellite primers that have been designed from sequencing of the Mexican spotted owl (*S. o. lucida*) (Thode et al. 2002) as well as additional primers that were designed from sequences obtained from other strigid (Aves: Strigidae) species (Isaksson and Tegelström 2002; Hsu et al. 2003, 2006; Koopman et al. 2004; Proudfoot et al. 2005), but which have been used in population-level studies of *S. occidentalis* (Funk et al. 2008, 2010) and/or have been found to be useful in genetically determining F1 and F2 *S. occidentalis* × *S. varia* hybrids (Funk et al. 2007). We searched the assembly for 16 pairs of microsatellite primer sequences using NCBI's BLAST+ version 2.4.0 tool BLASTN (Altschul et al. 1997; Camacho et al. 2009) (supplementary section 1.26, Supplementary Material online).

Barred Owl Divergence

In order to assess the genome-wide divergence of *S. occidentalis* and *S. varia*, we extracted genomic DNA from preserved tissue of a *S. varia* collected in Hamilton County, Ohio ([CNHM<USA-OH>:ORNITH:B41533]; hereafter referred to as "CMCB41533"; table 1) using a DNeasy Blood & Tissue Kit (Qiagen). We prepared a whole-genome library with an average insert length of 466 nt using a Nextera DNA Sample Preparation Kit (Illumina) and obtained 150 nt paired-end sequence data. We performed adapter and quality trimming of the sequence data using Trimmomatic version 0.32 (Bolger et al. 2014). We aligned the trimmed sequences to StrOccCau_1.0_masked using BWA-MEM version 0.7.12-r1044 (Li 2013a) and then merged the alignments, sorted the alignments, and marked duplicate sequences using Picard version 1.104 (http://broadinstitute.github.io/picard; last accessed October 1, 2016). We then calculated alignment statistics using Picard version 1.141 (http://broadinstitute.github.io/picard; last accessed October 1, 2016). We used Genome Analysis Toolkit (GATK) version 3.4-46 UnifiedGenotyper (McKenna et al. 2010; DePristo et al. 2011; Van der Auwera et al. 2013) to call variants using the *S. occidentalis* (Sequoia) and *S. varia* (CMCB41533) BWA-MEM-aligned, sorted, duplicate-marked bam files as simultaneous inputs (supplementary section 1.27, Supplementary Material online).

We then filtered the variants to exclude indels, sites of low genotyping quality, sites where the reference individual had a homozygous alternative allele genotype, and sites with coverage greater than the mean coverage plus five times the standard deviation, as suggested by the GATK documentation (https://software.broadinstitute.org/gatk/guide/article?id=3225; last accessed October 1, 2016). We used GNU cut version 8.21 (Ihnat et al. 2013) and GNU Awk (GAWK) version 4.0.1 (Free Software Foundation 2012) to calculate H_w, the mean number of nucleotide differences within *S. o. caurina* and *S. varia*, as well as H_b, the number of nucleotide differences between the two species, and then used these to estimate the fixation index (F_{ST}) (Hudson et al. 1992), a measure of population differentiation (supplementary section 1.27, Supplementary Material online). We then used an implementation of the pairwise sequentially Markovian coalescent model, PSMC version 0.6.5-r67 (Li and Durbin 2011; Li 2015), with 100 rounds of bootstrapping to estimate the effective population size (N_e) through time for both *S. o. caurina* and *S. varia* (supplementary section 1.28, Supplementary Material online).

Light-Associated Gene Analyses

We searched our *S. o. caurina* StrOccCau_1.0 assembly and the *T. alba* genome assembly (GenBank Accession GCA_000687205.1) for the presence of functional orthologs in nineteen genes that encode proteins with light-associated functions. These genes encode five visual

pigment proteins (*LWS* [long wavelength-sensitive opsin], *SWS1* [short wavelength-sensitive 1 opsin], *SWS2* [short wavelength-sensitive 2 opsin], *Rh1* [rod opsin], *Rh2* [rod-like cone opsin]) (Davies et al. 2012); ten nonvisual photopigment proteins (*Opn3* [panopsin/encephalopsin], *Opn4m* [mammal-like melanopsin], *Opn4x* [*Xenopus*-like melanopsin], *Opn5* [neuropsin], *Opn5L1* [neuropsin-like 1], *Opn5L2* [neuropsin-like 2], *OpnP* [pinopsin], *RRH* [peropsin], *RGR* [retinal G protein-coupled receptor], *OpnVA* [vertebrate ancient opsin]) (Okano et al. 1994; Shen et al. 1994; Soni and Foster 1997; Sun et al. 1997; Blackshaw and Snyder 1999; Halford et al. 2001; Tarttelin et al. 2003; Bellingham et al. 2006; Tomonari et al. 2008); three enzymes involved in protection from UV radiation (*EEVS*-like, *MT-Ox*, *pOPC1* [photolyase]) (Kato et al. 1994; Osborn et al. 2015); and an enzyme involved in synthesizing red ketocarotenoid pigments (*CYP2J19* [carotenoid ketolase]) (Lopes et al. 2016; Mundy et al. 2016). We queried the genome assemblies of *S. o. caurina* and *T. alba* utilizing *in silico* probes that encompassed the exons, introns and 5' and 3' flanking sequences of the above genes (see supplementary table S3, Supplementary Material online for details on the probe sequences). We imported the *S. o. caurina* genome assembly into Geneious version 9.1.6 (Kearse et al. 2012; Biomatters 2016b) and used the included version of the NCBI BLAST+ BLASTn tool (Zhang et al. 2000) to search for the probes in our assembly. We used the web version of NCBI BLAST+ version 2.5.0 (Zhang et al. 2000) to align the probes against the *T. alba* genome assembly sequences in the NCBI Whole-Genome-Shotgun (WGS) contigs database. After recovering matches with our BLAST searches, we used the Geneious version 9.1.6 implementation of the MUSCLE aligner (Edgar 2004) to align the BLAST results to the probe sequences. We then used Geneious version 9.1.6 to manually adjust the alignments and examine the owl sequences for inactivating mutations, such as premature stop codons, frame shift indels (insertions/deletions), and splice site mutations. When BLAST searches were unsuccessful, we performed BLAST searches against the discarded < 1,000 nt contig set. In cases of further negative results, we used synteny data from Ensembl (version 86; Yates et al. 2016) to search for evidence of whole gene deletion (supplementary section 1.29, Supplementary Material online and supplementary table S3, Supplementary Material online). Specifically, we identified genes flanking the gene of interest in other vertebrate taxa with available contiguous genomic sequence through the relevant region, and used BLAST as noted earlier to align the reference sequences for these flanking genes to the genome assemblies of *S. o. caurina* and *T. alba*. If both flanking genes occurred on the same contig/scaffold and the intergenic sequence was not composed of missing data (N's), this provided evidence that the gene of interest had been deleted from the genome. In order to provide further evidence of gene deletion, we used the web version of NCBI BLAST+ version 2.5.0 blastn tool (Zhang et al. 2000) to align the assembly sequence

intervening the flanking genes to available sequence data in the NCBI nucleotide database "nt" (Clark et al. 2016; NCBI Resource Coordinators 2016) to search for remnant sequences of untranslated gene regions.

In instances where we discovered evidence of potentially inactivating mutations in light-associated genes of one or both owl species, we performed dN/dS ratio (ω) analyses to test whether the owl orthologs displayed evidence of relaxation of the strength of natural selection. We obtained additional ortholog sequences for the following nonowl avian species using the web version of the NCBI BLAST+ version 2.5.0 blastn tool (Zhang et al. 2000) with the discontiguous megablast option to search the NCBI nucleotide database "nt" (Clark et al. 2016; NCBI Resource Coordinators 2016): *A. chrysaetos*, turkey vulture (*Cathartes aura*), speckled mousebird (*Colius striatus*), cuckoo roller (*Leptosomus discolor*), bar-tailed trogon (*Apaloderma vittatum*), rhinoceros hornbill (*Buceros rhinoceros*), downy woodpecker (*P. pubescens*), and the northern carmine bee-eater (*Merops nubicus*) (see supplementary table S9, Supplementary Material online for sequence information). After aligning the owl gene sequences with the outgroup taxa using MUSCLE (Edgar 2004) in Geneious version 9.1.6, we adjusted the alignments manually and removed all stop codons as well as any codon positions with questionable homology. We then modeled the evolution of the genes of interest using the codeml program from the PAML version 4.8 package (Yang 2007) assuming the Prum et al. (2015) phylogeny and two separate codon frequency models (F1X4 and F3X4). We created nested models and tested for statistically significant differences in model fits using likelihood ratio tests (parameters included model = 0 [one ratio] or 2 [nested models], fix_omega = 0, NSsites = 0, see supplementary tables S10 and S11, Supplementary Material online for additional information). Most models implemented branch tests, which assumed that ω differed across branches on the phylogeny, but was equal across a gene. We estimated the foreground ω on the *Tyto* branch for *OpnP*, the *Strix* and *Tyto* branches for *CYP2J19* and *Rh2*, and the crown (*Strix*+ *Tyto*) and stem Strigiformes branches for *Opn4m*. The background ω for each gene consisted of the remaining branches. In a few instances, we implemented branch-sites tests, which assumed differences in ω across the phylogeny while allowing for different ω values across different portions of a gene (parameters included model = 2, fix_omega = 1 [null] or 0 [alternative], omega = 1, NSsites = 2).

We additionally used the NCBI BLAST+ version 2.5.0 blastn tool (Zhang et al. 2000) with the discontiguous megablast option to align a reference *Opn4m* sequence to fifteen avian retinal transcriptomes, which included six owl species (Wu et al. 2016) in NCBI's Sequence Read Archive (SRA) (Leinonen et al. 2011; NCBI Resource Coordinators 2016) (see supplementary section 1.29, Supplementary Material online for additional transcriptome information). We imported

the short reads that aligned into Geneious version 9.1.6 (Kearse et al. 2012; Biomatters 2016b) and mapped them to the reference sequence using the Geneious "map to reference" function and trying both the "medium sensitivity/fast" and "low sensitivity/fastest" settings.

Results

Contamination Assessment

Our search for nonvertebrate sequences in our assembly suggested that our assembly was only very minimally contaminated with nonvertebrate sequences. For only nine out of the 8,113 final assembly scaffolds, one of the five top alignments to the NCBI nucleotide database (Clark et al. 2016; NCBI Resource Coordinators 2016) was an alignment to a nonvertebrate sequence. Four of these scaffolds were short, ranging from 1,182 to 2,304 nt, and aligned to *Escherichia coli* sequence data. We removed these four scaffolds from the assembly. We kept the other five scaffolds in the assembly. The highest BLAST bit-score for scaffold-1085 was for an alignment to the telomere region of a human genome with 81% identity across 53% of the scaffold. The highest BLAST bit-scores for scaffold-1155 were for alignments to endogenous retrovirus regions of several vertebrate genomes. Three scaffolds (2014, 2160, and 3069) were longer scaffolds that aligned to vertebrate genome sequences with only small sequence portions that aligned to nonvertebrate sequence data; we did not feel this justified removing them from the assembly.

Mitochondrial Genome Identification

We identified scaffold-3674 as an assembly of the mitochondrial genome as it had a 14,649 nt alignment with 89.1% similarity to the *S. leptogrammica* mitochondrial genome. This length was the majority of the 21,628 nt scaffold-3674. After subtracting a block of 3,984 N's present in the scaffold, the length of scaffold-3674 is similar to that of other avian mitochondrial genomes (Mindell et al. 1997, 1998, 1999; Guan et al. 2016; Zhang et al. 2016). We were able to annotate all of the standard avian mitochondrial genes, except *ND6* and *tRNA^Pro*, which suggests that this assembly of the mitochondrial genome could be improved.

Genome Size

Our *k*-mer-based estimation with Preqc yielded an estimated genome length of 1.29 giga nucleotides (Gnt). This type of estimation generally underestimates the true genome size as it collapses *k*-mers from highly repetitive regions. The total length of all sequences in our gap-closed assembly was 1.88 Gnt, but this length included all singleton sequences (many of which were unassembled reads) and N-filled gaps. After removing all contigs and scaffolds <1,000 nt, the combined total length of all scaffolds was 1.26 Gnt.

Assembly Statistics

Gap-closing improved the assembly continuity and completeness metrics (tables 3 and 4). Removing shorter length contigs/scaffolds improved the post gap closing assembly metrics at both the contig and the scaffold level. The unfiltered assembly had a scaffold N50 length of 1.836 Mnt and a contig N50 length of 81,400 nt. Removing contigs/scaffolds less than 300 nt increased the scaffold and contig N50 lengths over 2× to 3.916 Mnt and 168,721 nt, respectively, and generated the greatest relative increase in the other continuity metrics of any of the filtering options that we tried (supplementary table S4, Supplementary Material online). The highest scaffold and contig N50 lengths (3.983 Mnt and 171,882 nt, respectively) and the best other continuity metrics resulted from removing all contigs and scaffolds <1,000 nt, but this came at the slight expense of the completeness of the genome (supplementary table S4, Supplementary Material online; tables 3 and 4). Our gap-closed genome included complete sequences of 228 and at least partial sequences of 236 of the 248 CEGMA orthologs. We only lost one of these when we removed contigs and scaffolds <1,000 nt and retained 228 complete and 235 partial CEGMA orthologs in the filtered assembly (table 4). Except for the percentage of duplicated orthologs, which was notably higher as measured by the CEGMA analysis versus the BUSCO analysis, the results of the CEGMA and BUSCO analyses closely agreed. Both found at least partial sequences of over 90% of the conserved orthologs (235/248 = 94.76% CEGMA and 2,815/3,023 = 93.12% BUSCO orthologs) under scrutiny in the final assembly (table 4). Our final assembly contained 8,113 scaffolds and/or contigs with a scaffold N50 of 3.98 Mnt. The longest scaffold was 15.75 Mnt. The GC content was 41.31%. The N content was 1.10%.

The contig-level continuity statistics improved substantially when we allowed for longer blocks of intervening N's before demarcating separate contigs (supplementary table S4, Supplementary Material online). Relative to delineating contigs at every N (contig N50 of 51,301 nt), allowing up to 5 N's before demarcating a separate contig yielded an over 3× increase in the contig N50 of 155,200 nt. This was the greatest relative increase that we saw in the contig N50 length out of all the intervening N lengths that we tried, (supplementary table S4, Supplementary Material online). Allowing up to 25 N's before demarcating a separate contig resulted in the highest contig N50 (171.88 kilo nucleotides (knt); supplementary table S4, Supplementary Material online). In both continuity and completeness, our assembly compares favorably with those of the other avian genomes for which we calculated equivalent metrics (table 5).

Sex Identification

We determined from our assembly that the sequence came from the genome of a female *S. o. caurina*. The lengths of the *CHD1* markers on the sex chromosomes were 634 and 1,058 nt on scaffolds 806 and 4429, respectively. These lengths are in the size range of those amplified from *S. nebulosa* samples by previous researchers (600–650 and 1,200 nt for *CHD1Z* and *CHD1W*, respectively) (Fridolfsson and Ellegren 1999) and suggest that scaffolds 806 and 4429 are sequences from the Z and W chromosomes, respectively.

Repeat Annotation

The repeat annotation and masking of the genome examined 3,754,965 individual sequences totaling 1,882,109,172 nt. The homology-based repeat annotation resulted in GC content estimation of 44.15% and masked 21.02% of the assembly as repetitive. Repeat masking using a *de novo* model of the repeat elements estimated that an additional 0.55% of the assembly was repetitive. Due to the fact that some of the annotated repetitive elements overlapped, the following repeat category percentage values do not exactly sum to the 21.57% total genome repeat content. Interspersed repeat elements including retroelements, DNA elements (DNA transposons with no RNA intermediate), and unclassified elements comprised 9.31% of the assembly; of these, retroelements were the most common, constituting 8.96% of the assembly (table 6). Non-interspersed repeat elements including small RNA elements, satellites, simple repeats, and low complexity repeats comprised 12.33% of the assembly; of these, satellites were the most common, constituting 9.88% of the assembly.

Gene Annotation

The MAKER pipeline succeeded in annotating all contigs and scaffolds except one, scaffold-1363, which is 555,526 nt long and failed the annotation pipeline for an unknown reason. The MAKER pipeline's implementation of AUGUSTUS version 3.2.1 (Keller et al. 2011; Stanke 2015) predicted 19,692 proteins and transcripts *ab initio*. After quality filtering, we retained 16,718 annotated proteins and transcripts, 5,062 of which were non-overlapping *ab initio* predictions of proteins and transcripts.

Annotated gene sequence lengths ranged from 51 to 282,544 nt with a median length of 9,187.50 nt (supplementary fig. S2, Supplementary Material online). Coding sequence lengths varied from 51 to 66,303 nt with a median length of 1,137 nt (supplementary fig. S3, Supplementary Material online). Exon lengths extended to a maximum of 14,832 nt with a median length of 130 nt (supplementary fig. S4, Supplementary Material online). Intron lengths ranged from 45 to 57,529 nt with a median length of 910 nt (supplementary fig. S5, Supplementary Material online). The number of exons per gene ranged from 1 exon to 142 exons with a median number of six exons per gene (supplementary fig. S6, Supplementary Material online).

Alignment

The assembly contained 1,142, 612,682 nonN bases used in the calculation of the library alignment statistics. After all

Table 3

Final Assembly Metrics

Assembly Version	No Gap-Closing, no Scaffolds, or Contigs Removed	Gap-Closed, No Scaffolds or Contigs Removed	Gap-Closed, Scaffolds and Contigs <1,000 nt Removed
Number of scaffolds	3,754,960	3,754,960	8,108
Total size of scaffolds	1,884,397,264 nt	1,882,081,621 nt	1,255,541,132 nt
Longest scaffold	15,783,852 nt	15,750,186 nt	15,750,186 nt
Shortest scaffold	128 nt	128 nt	1,000 nt
Number of scaffolds > 1 K nt	8,112 (0.2%)	8,095 (0.2%)	8,095 (99.8%)
Number of scaffolds > 10 K nt	1,754 (0.0%)	1,746 (0.0%)	1,746 (21.5%)
Number of scaffolds > 100 K nt	661 (0.0%)	661 (0.0%)	661 (8.2%)
Number of scaffolds > 1 M nt	303 (0.0%)	303 (0.0%)	303 (3.7%)
Number of scaffolds > 10 M nt	9 (0.0%)	9 (0.0%)	9 (0.1%)
Mean scaffold size	502 nt	501 nt	154,852 nt
Median scaffold size	150 nt	150 nt	1,904 nt
N50 scaffold length (L50 scaffold count)	1,843,286 nt (209)	1,836,279 nt (209)	3,983,020 nt (92)
N60 scaffold length (L60 scaffold count)	622,124 nt (370)	619,581 nt (371)	3,012,707 nt (129)
N70 scaffold length (L70 scaffold count)	255 nt (216,251)	255 nt (218,976)	2,162,240 nt (178)
N80 scaffold length (L80 scaffold count)	174 nt (1,110,583)	174 nt (1,113,245)	1,545,070 nt (246)
N90 scaffold length (L90 scaffold count)	143 nt (2,336,958)	143 nt (2,338,577)	618,731 nt (372)
scaffold %GC	42.81%	43.82%	41.31%
scaffold %N	2.89%	0.74%	1.10%
Percentage of assembly in scaffolded contigs	66.4%	65.7%	98.5%
Percentage of assembly in unscaffolded contigs	33.6%	34.3%	1.5%
Average number of contigs per scaffold	1.0	1.0	3.4
Average length of break (>25 Ns) between contigs in scaffold	311	703	716
Number of contigs	3,929,029	3,774,552	27,252
Number of contigs in scaffolds	179,939	22,372	21,478
Number of contigs not in scaffolds	3,749,090	3,752,180	5,774
Total size of contigs	1,830,109,624 nt	1,868,296,631 nt	1,241,823,123 nt
Longest contig	186,255 nt	1,259,046 nt	1,259,046 nt
Shortest contig	5 nt	128 nt	130 nt
Number of contigs > 1 K nt	123,891 (3.2%)	23,915 (0.6%)	23,915 (87.8%)
Number of contigs > 10 K nt	37,347 (1.0%)	12,373 (0.3%)	12,373 (45.4%)
Number of contigs > 100 K nt	58 (0.0%)	3,909 (0.1%)	3,909 (14.3%)
Number of contigs > 1 M nt	0 (0.0%)	8 (0.0%)	8 (0.0%)
Mean contig size	466 nt	495 nt	45,568 nt
Median contig size	150 nt	150 nt	6,702 nt
N50 contig length (L50 contig count)	7,855 nt (46,856)	81,400 nt (4,678)	171,882 nt (2,057)
N60 contig length (L60 contig count)	3,275 nt (81,600)	33,521 nt (8,121)	134,419 nt (2,876)
N70 contig length (L70 contig count)	254 nt (448,715)	255 nt (254,729)	98,604 nt (3,955)
N80 contig length (L80 contig count)	170 nt (1,346,255)	173 nt (1,148,692)	66,668 nt (5,484)
N90 contig length (L90 contig count)	142 nt (2,548,877)	142 nt (2,367,845)	34,559 nt (8,023)

Note.—Assembly (contaminant and mitochondrial sequences removed) metrics before gap-closing, after gap-closing, and after both gap-closing and removal of all contigs and scaffolds <1,000 nt in length. Strings of 25 or more N's broke scaffolds into contigs.

filters, the total mean coverage for the paired and unpaired data from all of the sequenced libraries aligned to the repeat-masked genome was 60.43×. The MP11 kb mate-pair library had the highest proportion of duplicate bases (60.1%) and the PCR-free library noPCR550 bp had the lowest (0.3%) (table 7).

Insert sizes of mate pair libraries determined by mapping quality-filtered reads back to the genome assembly gave lower inserts than were expected based on bioanalyzer traces.

Whereas the bioanalyzer traces gave evidence that the MP4, MP7, and MP11 kb libraries had insert lengths of ~4.2, 7.1, and 10.7 knt, respectively, the results from mapping to the whole genome assembly suggested that the insert lengths were instead 3.3, 5.9, and 9.6 knt, respectively. We hypothesized that this difference may have been due to the number of N's added during scaffolding, we also mapped the sequences from these libraries to the assembly with all scaffolds decomposed into their constituent contigs. This yielded

Table 4

Summary of Conserved Ortholog Searches

Assembly	Draft. No Gap-Closing, Contigs/Scaffolds < 300 nt Removed	Draft. Gap-Closed, No Removal of Small Contigs/Scaffolds	Final. Gap-Closed, Contigs/Scaffolds <1,000 nt Removed	Final. Gap-Closed, Contigs/Scaffolds <1,000 nt Removed
Method	CEGMA	CEGMA	CEGMA	BUSCO
Total conserved orthologs examined	248	248	248	3,023
Complete orthologs (% of total)	221 (89.11%)	228 (91.94%)	228 (91.94%)	2,605 (86.17%)
At least partial orthologs (% of total)	235 (94.76%)	236 (95.16%)	235 (94.76%)	2,815 (93.12%)
Duplicated orthologs (% of total)	92 (37.10%)	83 (33.47%)	99 (39.92%)	46 (1.52%)
Missing orthologs	13 (5.24%)	12 (4.84%)	13 (5.24%)	208 (6.88%)

NOTE.—Comparison of the number of conserved orthologous genes found in the final assembly (gap-closed,contigs/scaffolds <1,000 nt removed) using the CEGMA and BUSCO tools. In order to illustrate the effect of gap-closing and removal of small fragments on assembly completeness metrics,also included are the results of CEGMA gene searches conducted on two draft versions of the final assembly where we either did not perform gap-closing and removed contigs/scaffolds < 300 nt or performed gap-closing and did not remove any small contigs/scaffolds.

Table 5

Comparative Statistics of Avian Genomes

Species	Common name	Scaffold N50 (nt)	No. Scaffolds/ Contigs	Contig N50 (nt)	Length (Gnt)	Ns (%)	Complete CEGs (% of 248)	Partial CEGs (% of 248)
S. o. caurina	Northern Spotted Owl	3,983,020	8,108	171,882	1.26	1.10	228 (91.94%)	235 (94.76%)
T. alba	Barn Owl	51,873	166,092	19,113	1.14	1.02	144 (58.06%)	198 (79.84%)
P. pubescens	Downy Woodpecker	2,086,781	85,828	29,578	1.17	3.72	196 (79.03%)	216 (87.10%)
T. guttata	Zebra Finch	62,374,962	37,095	38,644	1.23	0.75	192 (77.42%)	214 (86.29%)
H. leucocephalus	Bald Eagle	669,725	346,419	10,218	1.26	3.97	217 (87.50%)	240 (96.77%)
A. chrysaetos	Golden Eagle	9,230,743	1,141	215,151	1.19	1.07	226 (91.13%)	238 (95.97%)
C. pelagica	Chimney swift	3,839,435	60,234	33,918	1.13	4.02	191 (77.02%)	222 (89.52%)
G. gallus	Chicken	82,310,166	23,474	2,905,620	1.23	0.96	226 (91.13%)	237 (95.56%)

NOTE.—Comparative statistics of our S. o. caurina assembly with those of a selection of other avian genome assemblies.

average insert sizes of 3.3, 6.0, and 10.0 knt, which suggest some potential for improving N gap lengths, but that the N stretches in the scaffolds are good approximations of the lengths of missing, intervening sequences.

Microsatellite Analysis

We found 15 out of the 16 pairs of microsatellite primers for which we searched in the genome assembly (table 8). We found loci 4E10, 4E10.2, and Oe149 on scaffold-11. The distance from the forward 4E10.2 primer to the forward 4E10 primer is 12,172 nt in our assembly, which confirms the characterization of the loci 4E10 and 4E10.2 as linked within 40 kb by the original authors who described these loci using sequences obtained from the same cosmid (Thode et al. 2002). The reverse 4E10 primer is 717,153 nt distant from the forward Oe149 primer. The remaining primer pairs aligned to separate assembly scaffolds (table 8).

Barred Owl Divergence

We estimated the nuclear genome-wide nucleotide diversity (H_W) of S. o. caurina as 2.008×10^{-4} and that of S. varia as 2.352×10^{-3}. We estimated the genome-wide nucleotide

diversity between S. o. caurina and S. varia (H_b) as 7.042×10^{-3} and calculated an F_{ST} of 0.819.

PSMC Analysis

Our pairwise sequentially Markovian coalescent (PSMC) model analyses suggested that the N_e of both S. o. caurina and S. varia was substantially higher in the past and has been in decline since ∼100,000 or 80,000 years before present, respectively (fig. 1). The estimated peak N_e of S. o. caurina was more than an order of magnitude lower than that of S. varia (∼20,000 and 250,000 for S. o. caurina and S. varia, respectively). The most recent estimate that the PSMC analysis provided for the N_e of S. o. caurina was also more than an order of magnitude lower than that of S. varia (∼4,000 and 50,000 for S. o. caurina and S. varia, respectively).

Light-Associated Gene Analyses

Seven of the nineteen genes encoding proteins with light-associated functions that we examined displayed evidence of inactivation or whole gene deletion in one or both owl species (supplementary table S3, Supplementary Material online; Hanna et al. 2017). We found no BLAST alignments of

Table 6

Repetitive Element Summary

Type Level 1	Type Level 2	Type Level 3	Type Level 4	Number of Elements	Element Total Length (nt)	Assembly Portion (%)
Total interspersed repeats					175,287,790	9.31
	Total retroelements			727,006	168,672,903	8.96
	Retroelement	SINE		40,360	4,770,020	0.25
	Retroelement	SINE	ALU	53	6,194	0.00
	Retroelement	SINE	MIR	15,510	1,558,420	0.08
	Retroelement	Penelope		169	35,110	0.00
	Retroelement	Total LINEs		486,310	115,604,290	6.14
	Retroelement	LINE	LINE1	622	58,117	0.00
	Retroelement	LINE	LINE2	3,116	317,864	0.02
	Retroelement	LINE	L3/CR1	28,122	5,153,289	0.27
	Retroelement	LINE	CRE/SLACS	0	0	0.00
	Retroelement	LINE	L2/CR1/Rex	452,030	109,807,316	5.83
	Retroelement	LINE	R1/LOA/Jockey	0	0	0.00
	Retroelement	LINE	R2/R4/NeSL	131	44,590	0.00
	Retroelement	LINE	RTE/Bov-B	15	3,492	0.00
	Retroelement	LINE	L1/CIN4	98	23,441	0.00
	Retroelement	Total LTR elements		200,336	48,298,593	2.57
	Retroelement	LTR	BEL/Pao	0	0	0.00
	Retroelement	LTR	ERV_classI	983	122,219	0.01
	Retroelement	LTR	ERV_classII	400	54,854	0.00
	Retroelement	LTR	ERVL	436	91,660	0.00
	Retroelement	LTR	ERVL-MaLRs	51	4,838	0.00
	Retroelement	LTR	Gypsy/DIRS1	111	14,921	0.00
	Retroelement	LTR	Retroviral	197,967	47,947,799	2.55
	Retroelement	LTR	Ty1/Copia	0	0	0.00
	Total DNA elements			37,526	5,628,486	0.30
	DNA element		En-Spm	0	0	0.00
	DNA element		hAT-Charlie	418	28,220	0.00
	DNA element		hobo-Activator	4,235	719,417	0.04
	DNA element		MuDR-IS905	0	0	0.00
	DNA element		PiggyBac	0	0	0.00
	DNA element		Tc1-IS630-Pogo	806	141,663	0.01
	DNA element		TcMar-Tigger	528	39,074	0.00
	DNA element		Tourist/Harbinger	9,255	958,360	0.05
	DNA element		Other (Mirage, P-element,Transib)	0	0	0.00
	Rolling-circles			0	0	0.00
	Unclassified interspersed repeats			6,225	986,401	0.05
Total noninterspersed repeats				1,907,394	232,038,709	12.33
	Small RNA			12,051	1,645,166	0.09
	Satellites			1,261,021	185,995,538	9.88
	Simple repeats			564,508	40,568,395	2.16
	Low complexity repeats			69,814	3,829,610	0.20

NOTE.—Summary of the repeat elements found during two rounds of repeat masking (homology-based followed by denovo-model-based masking). Depending on the type of repeat element, we provide information at different category summary levels. We use the "Type level" column headings to organize these categories.

SWS1 to either the *S. o. caurina* or the *T. alba* assembly. However, the genes flanking *SWS1* in zebra finch (*T. guttata*) and human (*Homo sapiens*), *FLNC* (Filamin-C) and *CALU* (Calumenin) (Ensembl version 86; Yates et al. 2016), are both present in the *S. o. caurina* genome assembly, but they are located on different scaffolds. Without increased genomic continuity, it is difficult to discern whether

chromosomal rearrangement has occurred or whether this is a case of simple gene deletion. Recent searches in crocodilian (Crocodilia) genomes similarly found *FLNC* and *CALU* on separate contigs with *SWS1* missing from the assemblies (Emerling 2017a), which suggests that this may be a problematic region to assemble. NCBI's Eukaryotic Genome Annotation (EGA) pipeline did not find *FLNC* and *CALU* in

Table 7
Library Alignment Statistics

Library	Mean Paired and Unpaired Read Genome Coverage Postfiltering (X)	SD of Paired and Unpaired Read Genome Coverage Postfiltering (X)	Fraction of Aligned Bases From Unpaired Reads	Total Fraction of Filtered Aligned Bases	Fraction Aligned Bases Filtered Due to Mapping Quality < 20	Fraction Aligned Bases Filtered as Duplicates	Fraction Aligned Bases Filtered as Low Quality With Q<20	Fraction Aligned Bases Filtered as Second Observation From Overlapping Reads	Fraction Aligned Bases Filtered From Regions Already with > 1,000× coverage
Nextera350bp lane 1	4.369	5.484	0.048	0.533	0.060	0.444	0.004	0.023	1.52E-03
Nextera350bp lane 2	11.162	8.960	0.039	0.559	0.056	0.480	0.005	0.017	1.43E-03
Hydroshear	1.093	2.784	0.004	0.549	0.033	0.429	0.005	0.081	2.03E-03
Nextera550bp lane 1	2.741	3.708	0.393	0.096	0.034	0.038	0.011	0.011	1.05E-03
Nextera550bp lane 2	5.790	5.435	0.327	0.126	0.032	0.066	0.019	0.008	1.26E-03
Nextera700bp	23.357	14.710	0.041	0.216	0.046	0.126	0.009	0.032	3.64E-03
noPCR550bp	3.244	2.661	0.241	0.059	0.013	0.003	0.014	0.029	4.32E-04
PCR900bp	1.978	1.894	0.073	0.052	0.012	0.024	0.014	0.001	3.34E-04
MP4kb	2.528	2.745	0.300	0.361	0.048	0.306	0.002	0.004	5.36E-04
MP7kb	2.528	2.734	0.256	0.449	0.045	0.397	0.002	0.004	4.53E-04
MP11kb	1.641	2.205	0.168	0.652	0.046	0.601	0.001	0.004	2.56E-04
CMCB41533	15.552	12.253	0.030	0.341	0.299	0.037	2.37E-04	2.59E-03	2.50E-03

NOTE.—Alignment statistics for all Sequoia (*Strix occidentalis caurina*) libraries and the CMCB41533 (*Strix varia*) library calculated using Picard's CollectWgsMetrics.

the *T. alba* genome assembly (NCBI *T. alba* Annotation Release 100; NCBI Accession GCF_000687205.1), but the absence of these genes in the assembly may be due to low assembly quality (Zhang, Li B, Li C, et al. 2014).

SWS2 and *LWS* are adjacent on the same chromosome in the Carolina anole (*Anolis carolinensis*) and African clawed frog (*Xenopus laevis*) genome assemblies and are flanked by *MECP2* (methyl-CpG binding protein 2) in *A. carolinensis* and *X. laevis*, *AVPR2* (arginine vasopressin receptor 2) in *X. laevis*, and *TEX28* (testis expressed 28) in *A. carolinensis* (Ensembl version 86; Yates et al. 2016). We did not obtain BLAST alignments to *SWS2* or *LWS* for the *T. alba* assembly and NCBI's EGA pipeline did not find *MECP2*, *AVPR2*, or *TEX28* (NCBI *T. alba* Annotation Release 100; NCBI Accession GCF_000687205.1), which suggests that this portion of the genome, like the *SWS1* region, may be challenging to assemble. Although we found *SWS2* and *LWS* in our *S. o. caurina* assembly, we only obtained partial coding sequences with elevated GC content of 66.9% and 68.0%, respectively. Our *S. o. caurina* assembly contained a partial *SWS2* exon 1 sequence as well as complete exon 2 and 3 sequences with all three exons found on two separate scaffolds (scaffolds 4153 and 7110). The sequences of these exons on the two scaffolds were 100% identical except for one difference in exon 3. Given the high sequence similarity and the recovery of the same portions of the *SWS2* coding region, these duplicate sequences are likely an artifact of the assembly process and do not indicate gene duplication.

SWS2, *LWS*, *Rh1*, and *Rh2* in *S. o. caurina* and *Rh1* in *T. alba* showed no evidence of potentially inactivating mutations. However, *Rh2* in *T. alba* displayed a 29 nt deletion in exon 1, single premature stop codons in both exons 2 and 3, and a 2 nt deletion in exon 4. Our modeling of the sequence evolution of *Rh2* in *S. o. caurina* and *T. alba* yielded evidence that selection has become relaxed in *T. alba* ($\omega = 0.22$–0.37; $P < 0.00001$) relative to other avian taxa ($\omega = 0.03$–0.06), which is consistent with pseudogenization of this gene. A branch test of *S. o. caurina* also displayed evidence of relaxed selection on *Rh2* with an elevated ω (0.16–0.21; $P < 0.05$) relative to the background. Our branch-sites test evaluated whether there was indication of positive selection across a subset of sites, but it did not yield any evidence that the elevated ω was due to adaptive evolution. We did find nine missense mutations in *S. o. caurina* that were not found in any of the non-owl avian species, but none of these were at known conserved sites (Carleton et al. 2005), which suggests that they have not resulted in a loss of function.

We were unable to recover *OpnP* in our *S. o. caurina* assembly, but together on the same scaffold we found the genes that flank *OpnP* in the chicken (*G. gallus*) and the collared flycatcher (*Ficedula albicollis*) genome assemblies, *TEX14* (testis expressed sequence 14) in *G. gallus* and *DOC2B* (double C2 domain beta) in *G. gallus* and *F. albicollis* (Ensembl version 86; Yates et al. 2016). Our BLAST of the sequence

Table 8

Genomic Locations of Selected Microsatellite Loci

Locus	Primer	References	Usage Comments	Length Primer	Length Alignment	Mismatches	Genome Scaffold	Genome Start	Genome End	Microsatellite Length (nt)
13D8	F	(Thode et al. 2002)	population genetics (Funk et al. 2008, 2010)	22	22	0	scaffold88	4,241,040	4,241,019	187
13D8	R			21	21	0	scaffold88	4,240,854	4,240,874	
15A6	F	(Thode et al. 2002)	population genetics (Funk et al. 2008, 2010)	21	21	0	scaffold233	2,208,703	2,208,723	148
15A6	R			19	16	0	scaffold233	2,208,847	2,208,832	
1C6	F	(Thode et al. 2002)	None	20	20	0	scaffold178	2,550,734	2,550,753	110
1C6	R			20	20	0	scaffold178	2,550,843	2,550,824	
4E10	F	(Thode et al. 2002)	None	22	22	0	scaffold11	768,391	768,371	230
4E10	R			22	22	0	scaffold11	768,162	768,183	
4E10.2	F	(Thode et al. 2002)	population genetics (Funk et al. 2008, 2010)	18	18	0	scaffold11	780,562	780,579	226
4E10.2	R			18	18	0	scaffold11	780,787	780,770	
6H8	F	(Thode et al. 2002)	population genetics (Funk et al. 2008, 2010)	21	21	0	scaffold103	3,773,885	3,773,865	93
6H8	R			16	16	0	scaffold103	3,773,793	3,773,808	
8G11	F	(Thode et al. 2002)	None	18	—	—	—	—	—	—
8G11	R			17	—	—	—	—	—	
Bb126	F	(Isaksson & Tegelström 2002)	hybrid diagnostic (Funk et al. 2007)	20	20	0	scaffold219	2,548,147	2,548,166	185
Bb126	R			24	24	0	scaffold219	2,548,331	2,548,308	
BOOW18	F	(Koopman et al. 2004)	hybrid diagnostic (Funk et al. 2007)	19	19	1	scaffold244	648,444	648,426	205
BOOW18	R			20	20	1	scaffold244	648,240	648,259	
FEPO5	F	(Proudfoot et al. 2005)	population genetics (Funk et al. 2008, 2010)	22	22	0	scaffold138	720,315	720,336	270
FEPO5	R			25	25	2	scaffold138	720,584	720,560	
Oe045	F	(Hsu et al. 2003)	hybrid diagnostic (Funk et al. 2007)	23	23	2	scaffold173	3,777,655	3,777,677	127
Oe045	R			19	19	0	scaffold173	3,777,781	3,777,763	
Oe053	F	(Hsu et al. 2003)	population genetics (Funk et al. 2008, 2010)	23	23	1	scaffold136	299,240	299,262	218
Oe053	R			22	22	1	scaffold136	299,457	299,436	
Oe128	F	(Hsu et al. 2003)	hybrid diagnostic (Funk et al. 2007), population genetics (Funk et al. 2008, 2010)	27	27	0	scaffold722	802,232	802,206	319
Oe128	R			24	24	0	scaffold722	801,914	801,937	
Oe129	F	(Hsu et al. 2006)	population genetics (Funk et al. 2008, 2010)	24	21	2	scaffold529	3,066,759	3,066,739	266

(continued)

Table 8 Continued

Locus	Primer	References	Usage Comments	Length Primer	Length Alignment	Mismatches	Genome Scaffold	Genome Start	Genome End	Microsatellite Length (nt)
Oe129	R			24	24	1	scaffold529	3,066,497	3,066,520	
Oe149	F	(Hsu et al. 2006)	population genetics (Funk et al. 2008, 2010)	21	21	1	scaffold11	51,010	50,990	258
Oe149	R			20	20	0	scaffold11	50,753	50,772	
Oe3-7	F	(Hsu et al. 2003)	population genetics (Funk et al. 2008, 2010)	20	19	1	scaffold35	572,329	572,347	129
Oe3-7	R			23	23	0	scaffold35	572,456	572,434	

NOTE.—Locations of commonly used microsatellite loci in our draft genome assembly. We searched for all of the primer pairs used in several *S. occidentalis* population genetics studies as well all of those designed for use in *S. o. lucida* (Thode et al. 2002). The "Primer" column designates the forward or reverse primer with "F" or "R," respectively. The "Reference" column gives the citation of the publication that originally described each primer pair. The "Comment" column gives the citation(s) of the publication(s) in which a primer pair has been used for population-level study of *S. occidentalis* or and/or study of *S. occidentalis x S. varia* hybrids. "Length alignment" refers to the length of the BLASTN (Altschul et al. 1997; Camacho et al. 2009) alignment. The "Microsatellite length" refers to the inferred length of the microsatellite PCR product based on the length of the primers and their mapping positions in the genome assembly.

intervening *TEX14* and *DOC2B* in our *S. o. caurina* assembly revealed similarity (8% query coverage, 82% identity) with the 5′ untranslated region of *G. gallus OpnP*. Together, these provide strong evidence of whole gene deletion of *OpnP* in *S. o. caurina*. *OpnP* in *T. alba* is a pseudogene with numerous inactivating mutations, including the following: a start codon mutation (ACA), 13 nt deletion, 2 nt insertion, and 1 nt deletion in exon 1, a 1 nt deletion in exon 2, a 21 nt deletion of the intron 3-exon 4 boundary, a 7 nt deletion and 2 nt deletion in exon 4, and a 1 nt deletion in exon 5. We assembled sequences from outgroup taxa and confirmed that these mutations are unique to *T. alba*. Our dN/dS ratio analyses strongly suggested relaxed selection on the *T. alba* branch ($\omega = 0.51–0.7$; $P < 0.00001$) compared with purifying selection on the background branches ($\omega = 0.11–0.18$).

Opn4m displays evidence of inactivation in both *S. o. caurina* and *T. alba*, with both species sharing a 4 nt deletion in exon 8. Additionally, *S. o. caurina* has a premature stop codon in exon 8 and *T. alba* possesses a splice donor mutation (GT to AT) in intron 11. Comparisons with outgroup taxa confirmed that these mutations were unique to owls, but also demonstrated that other bird species have putative inactivating mutations in this gene, including the golden eagle (*A. chrysaetos*) with a premature stop codon in exon 9; speckled mousebird (*C. striatus*) with a 1 nt deletion in exon 9, splice donor mutation in intron 9 (GT to TT), and premature stop codon exon 11; cuckoo roller (*L. discolor*) with a splice donor mutation in intron 10 (GT to GA); and rhinoceros hornbill (*B. rhinoceros*) with a start codon mutation (ATG to CTG). We performed dN/dS ratio analyses after removing all exons that contained putative inactivating mutations. The results indicated that the average ω for the crown owl branches is elevated ($\omega = 0.45$; $P < 0.01$) relative to the background ($\omega = 0.19$), which does not meet the expectation of neutral evolution predicted if the shared 4 nt deletion led to a loss of function of *Opn4m*. Branch-sites tests yielded evidence of positive selection on some portions of the gene for both owl branches, but this signal was not a significantly better fit than the null. Our BLAST of an *Opn4m* sequence to fifteen bird retinal mRNA short read databases, which included data from six owl species, yielded alignments to all fifteen transcriptomes. Further investigation of these sequences in Geneious revealed evidence of different isoforms of *Opn4m*. When we used lower sensitivity alignment settings, the assemblies of mapped sequences generally terminated after exon 8 (the exon with the 4 nt deletion), suggesting that this is an abundant transcript isoform. However, using higher sensitivity alignment settings generated assemblies of multiple transcripts with distinct sequences at some of the exon–intron boundaries.

Finally, *CYP2J19* displays evidence of inactivation in both owl species. *S. o. caurina* has a 1 nt insertion and 2 nt deletion in exon 9. As Emerling (2017c) described, the *T. alba* assembly contains a premature stop codon in each of exons 1, 5, and 6 as well as a 5 nt deletion in exon 3. Both the *S. o. caurina*
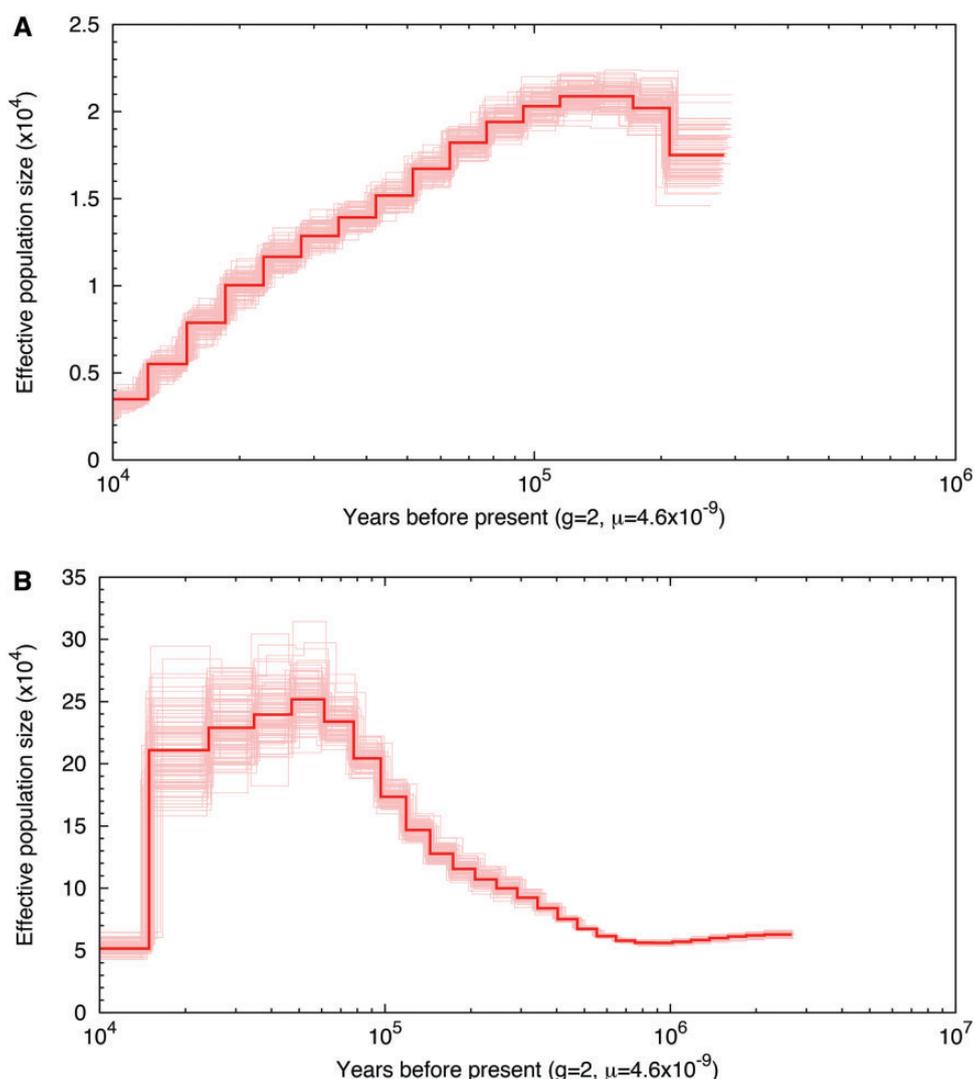
Fig. 1—Demographic history of *Strix occidentalis caurina* and *Strix varia* with bootstrap replicates. (Panel A) depicts the demographic history estimated for *S. o. caurina*. (Panel B) depicts the demographic history estimated for *Strix varia*.

($\omega = 0.33$–0.34; $P < 0.05$) and *T. alba* ($\omega = 0.68$–0.72; $P < 0.0001$) branches have elevated dN/dS ratios compared with the background (0.15–0.16), which is consistent with the hypothesis that these mutations have led to a loss of function of *CYP2J19*.

Discussion

Genome Characterization

Direct comparison of assembly metrics between our *S. o. caurina* assembly and seven other avian genome assemblies, including the avian model organisms chicken (*G. gallus*) and zebra finch (*T. guttata*), revealed that the *S. o. caurina* assembly is in the top tier of genomes in both continuity and completeness (table 5). Only the golden eagle (*A. chrysaetos*), zebra finch, and chicken genomes had better continuity

statistics as measured by scaffold and contig N50s. We compared the relative completeness of the assemblies by searching for a set of 248 CEGs using CEGMA. Of the assemblies that we compared, we found the highest number of complete conserved gene sequences in our *S. o. caurina* assembly (228 complete CEGs), surprisingly surpassing even the chicken genome (226 complete CEGs). In terms of at least partially complete sequences of conserved genes, our *S. o. caurina* assembly contained only two fewer than the chicken genome (235 vs. 237 partial CEGs). Our assembly is both more complete and more contiguous than that of *T. alba*, the only other owl assembly currently available (*S. o. caurina* vs. *T. alba* assembly statistics include 235 vs. 198 CEGs at least partially present, scaffold N50 of $\sim 4.0 \times 10^6$ nucleotides vs. $\sim 5.2 \times 10^4$ nucleotides, and contig N50 of $\sim 1.7 \times 10^5$ nucleotides vs. $\sim 1.9 \times 10^4$ nucleotides).

The number of annotated genes and the percentage of interspersed repeat elements in our *S. o. caurina* assembly are similar to those seen in other avian genomes (Zhang, Li B, Li C, et al. 2014). The number of annotated genes in our assembly (16,718 genes) was very similar to the number in the high-quality chicken and zebra finch genomes (16,516 and 17,471 genes, respectively) (Zhang, Li B, Li C, et al. 2014). These values were at the upper end of the range seen in the analysis of the gene annotations of 48 avian genomes (13,454–17,471 genes) (Zhang, Li B, Li C, et al. 2014). Similar to the number of annotated genes, the percentage of interspersed repeat elements in our *S. o. caurina* assembly (9.31%) closely matched the percentage found in the chicken and zebra finch genomes (9.82% and 9.68%, respectively) (Zhang, Li B, Li C, et al. 2014). These values fell at the higher end of the range seen in the analysis of 48 avian genomes (4.11–9.82%) if one excludes the downy woodpecker (*P. pubescens*) outlier (22.15%) (Zhang, Li B, Li C, et al. 2014).

Our searches for CEGs with both our CEGMA and BUSCO analyses revealed that our *S. o. caurina* assembly lacks only 5–7% of conserved orthologs, which is similar to the 4.4% we observed to be absent in the assembly of the chicken genome. Genome size data estimated from flow cytometry measurement of red blood cells exist for two *S. occidentalis* congeners. The nuclear genome lengths of the tawny owl (*Strix aluco*) and the great gray owl (*S. nebulosa*) are ~1.56 Gnt (De Vita et al. 1994; Doležel et al. 2003) and 1.61 Gnt (Doležel et al. 2003; Vinogradov 2005), respectively, which average to 1.59 Gnt. As compared with this average, the shorter total length of our scaffolded *S. o. caurina* assembly (~1.26 Gnt) suggests that 21% of the full genome sequence length of *S. o. caurina* remains unrepresented in this assembly. This is similar to the ~17.8% unrepresented sequence in the 1.19 Gnt golden eagle genome, assuming a genome size of ~1.45 Gnt (Doležel et al. 2003; Nakamura et al. 1990). The unrepresented sequence may consist largely of difficult-to-assemble repetitive content (Wicker et al. 2005; Yamada et al. 2004). These data illustrate that the *S. o caurina* assembly is comparable to the top tier of avian genomes assembled to date, but, as with all avian genomes, there is still improvement to be made.

Previous work on *Strix* karyotypes suggests that *S. occidentalis* likely has a typical avian karyotype of 2n = 80–82 (Renzoni and Vegni-Talluri 1966; Hammar 1970; Belterman and Boer 1984; Rebholz et al. 1993;). Assuming 1n = 41 chromosomes, the 8,100 scaffolds in our assembly yield ~198 scaffolds per chromosome. However, this number may not be a very meaningful estimate of the number of sequence blocks per chromosome as *Strix* shares with other birds the feature of possessing chromosomes in a wide range of sizes with the majority of the karyotype (~35 of the 41 chromosomes) comprised of microchromosomes and just 6 macrochromosomes (Rebholz et al. 1993).

The SOAPdenovo2 version 2.04 (Luo et al. 2012) assembler does not remove short sequences, which were mostly unincorporated reads. We removed all contigs and scaffolds <1,000 nt for our final assembly and used the resulting assembly in downstream analyses. We felt that removal of these small sequences was warranted as sequences shorter than 1,000 nt are unlikely to be useful in assessing synteny or gene structure. Some commonly used assemblers, such as ALLPATHS-LG, do not output contigs/scaffolds <1,000 nt (Gnerre et al. 2011). Indeed, the authors of the ALLPATHS-LG description removed contigs/scaffolds <1,000 nt in the comparisons of their assembler's functionality with other genome assemblers (Gnerre et al. 2011). Removal of these short sequences post assembly allowed us to better compare across assemblies and to effectively analyze what was actually assembled.

Our CEGMA results suggest that we lost minimal genome information (only 1 out of 248 conserved orthologs examined) by removing assembly contigs/scaffolds <1,000 nt. This validated our decision to remove these short sequences and confirmed that it was likely not worth the increase in processing time to retain these small genome fragments in downstream analyses. Additionally, larger genome assembly fragments have greater structural information.

In order to calculate the contig N50 statistic, scaffolds must be decomposed into constituent contigs. We explored how the criteria for splitting scaffolds into contigs affected assembly statistics. As one might expect, allowing longer blocks of N's before breaking a scaffold into contigs resulted in better continuity statistic values. We chose to allow up to 25 N's before separating contigs in our final assembly metric calculations as this was the default used in the "assemblathon_stats.pl" script used for calculating assembly statistics of the Assemblathon 2 genome assemblies (Bradnam et al. 2013). Indeed, even though the "assemblathon_stats.pl" script allowed the user to set a flag to change the number of N's that would separate contigs, our examination of the code revealed that the 25 N's was actually hard-coded into the script and overrode any value set by the user.

We found that our assemblies had better continuity metrics when we did not include all of our available short read data in the assembly. Of particular benefit was the exclusion of the Hydroshear data set, which displayed a high level of sequence duplication. This suggests that checking libraries for evidence of elevated levels of duplication prior to an assembly could be beneficial.

We found that all of the microsatellite primer pairs previously used for *S. occidentalis* genetic studies (Funk et al. 2007, 2008, 2010) mapped at reasonable distances from each other and predicted PCR products in normal microsatellite size ranges. We found no evidence of linkage except for three primer pairs that mapped to the same scaffold. The other 11 primer sets that we were able to align to the assembly

mapped to separate scaffolds. A chromosome-level genomic sequence assembly would help further evaluate the independence of these loci.

Genome-Wide Divergence of Spotted Owl and Barred Owl

As *S. o. caurina* and *S. varia* are separate species, we expected a high genome-wide F_{ST} estimate, but our estimate is elevated even relative to values calculated for other congeneric bird species pairs (Toews et al. 2016). It is difficult to interpret this value; however, as the genome-wide nucleotide diversity within *S. varia* is ~10-fold greater than that of *S. o. caurina*. We hypothesize that a difference in N_e for the two species is likely the largest contributor to this difference in nucleotide diversity, especially as the Marin *S. o. caurina* population of which our *S. o. caurina* genome is a sample is known to be an isolated population of this extinction-threatened species (Barrowclough et al. 2005). Following from the 10-fold difference in nucleotide diversity of the two species' genomes, our PSMC analyses suggested that the N_e of *S. varia* was consistently approximately an order of magnitude greater than that of *S. o. caurina* over the past 100,000 years. The PSMC analyses also suggested that the N_e of both *S. o. caurina* and *S. varia* has been in decline over the past tens of millennia, but we caution that precise timing of the past maximum N_e for both species and its subsequent decline is highly dependent on the values chosen for the substitution rate and generation time, which likely require further optimization for these *Strix* species and for owls in general.

Light-Associated Gene Analyses

We have provided genomic evidence of inactivation and deletion of genes with light-associated functions in two species of predominantly nocturnal owls. Ancestral birds likely possessed tetrachromatic color vision (Borges et al. 2015) characterized by four cone photoreceptor opsin pigments with distinct spectral sensitivities, but it appears that owls have a reduced capacity to discriminate colors. Our genomic data for the color vision system in owls are largely consistent with the results of a retinal microspectrophotometry study (Bowmaker and Martin 1978), retinal transcriptome analyses (Wu et al. 2016), and a recent genomic study of avian visual opsins (Borges et al. 2015). Specifically, the absence of *SWS1*, which absorbs light in the violet/ultraviolet (Davies et al. 2012), in both *S. o. caurina* and *T. alba* is corroborated by the absence of a violet/ultraviolet-sensitive photopigment in *S. aluco* (Bowmaker and Martin 1978), the lack of *SWS1* retinal mRNA transcripts in a tytonid and species from all three of the strigid subfamilies (Wu et al. 2016), and a genomic analysis of *T. alba* that also failed to find *SWS1* in the genome assembly (Borges et al. 2015). In our *S. o. caurina* assembly we were able to locate, albeit on separate scaffolds, the genes that flank *SWS1* in other avian taxa, but not *SWS1* itself. More data is needed to confirm whether there are *SWS1* remnants

in the *S. o. caurina* and *T. alba* genomes and their absence in the current assemblies is simply due to assembly incompleteness or errors. However, together the data accumulated to date strongly indicate that owls lack *SWS1*, potentially since their most recent common ancestor, leading to a reduced capacity for color discrimination. The loss of *SWS1* is highly unusual in Aves (Borges et al. 2015). Other than in owls, it has only been inferred to have been lost in the nocturnal North Island brown kiwi (*Apteryx mantelli*) (Le Duc et al. 2015). In contrast, it has occurred repeatedly in nocturnal, subterranean, and marine mammals (Jacobs 2013; Emerling et al. 2015) as well as in the crocodilians, a lineage believed to have undergone an extensive period of nocturnal adaptation (Walls 1942; Emerling 2017a).

The inactivation of *Rh2* in *T. alba* was previously suggested (Borges et al. 2015) and we confirmed this result with the two premature stop codons and two frameshift indels we found in the gene sequence. Additionally, there is evidence that the retinal transcriptome of a congener, *T. longimembris*, does not include *Rh2* transcripts (Wu et al. 2016). The intact copy of *Rh2* in our *S. o. caurina* genome, the transcription of this gene in multiple strigid species (Wu et al. 2016), and the expression of a cone pigment consistent with the Rh2 protein in *S. aluco* (Bowmaker and Martin 1978) all support the hypothesis that *Rh2* was lost uniquely in the tytonid lineage and not across Strigiformes (Wu et al. 2016). Among avian species, *Rh2* is also inactivated in the kiwi *A. mantelli* (Le Duc et al. 2015) as well as in the Adélie (*Pygoscelis adeliae*) and emperor penguins (*Aptenodytes forsteri*) (Li et al. 2014; Borges et al. 2015), two marine predators that frequently feed at great depths under dim-light conditions. A third penguin species, the Humboldt penguin (*Spheniscus humboldti*) lacks cones with a peak absorbance typical of *Rh2* (Bowmaker and Martin 1985). The loss of *Rh2* occurred in several other vertebrate groups that are thought to have experienced long periods of inhabiting dim-light environments, including stem Mammalia (Walls 1942; Davies et al. 2007; Gerkema et al. 2013), Crocodilia (Emerling 2017a), and snakes (Reptilia: Serpentes) (Castoe et al. 2013; Vonk et al. 2013; Simões et al. 2015; Emerling 2017b).

The apparent absence of *SWS2* and *LWS* in *T. alba* is likely due to the assembly being incomplete. These genes are in tandem in *A. carolinensis* and *X. laevis*, but the avian assemblies in Ensembl version 86 (Yates et al. 2016) contain *SWS2* and *LWS* on separate small contigs and not adjacent to other genes. This is consistent with our recovery of only partial *SWS2* and *LWS* in *S. o. caurina* and previous difficulties in assembling full *SWS2* and *LWS* sequences in dozens of other avian genomes (Borges et al. 2015; Le Duc et al. 2015), which may be attributable to the high GC content of these genes (Borges et al. 2015). Researchers recovered intact *SWS2* and *LWS* mRNAs in the retinal transcriptomes of five strigid and one tytonid species (Wu et al. 2016) and have demonstrated that the tawny owl (*S. aluco*) expresses photoreceptor

pigments with peak absorptions consistent with *SWS2* and *LWS* (Bowmaker and Martin 1978), suggesting that *SWS2* and *LWS* are likely retained in owls.

Together, the confluence of data from genomics, transcriptomics, and retinal microspectrophotometry suggests that *SWS1* was likely lost in stem Strigiformes, which resulted in a reduction in the degree of color vision from tetrachromacy to trichomacy by the time of the last common ancestor of owls. *Rh2* became subsequently inactivated in Tytonidae, resulting in further reduced capacity for color discrimination (dichromacy) in this family. Owls, kiwis, and penguins represent the few known avian taxa that deviated from the ancestral avian state of tetrachromatic color vision, likely as a result of an increased dependence on highly sensitive rod photoreceptors for foraging in low-light conditions.

The inactivation (*T. alba*) or deletion (*S. o. caurina*) of the gene encoding pinopsin (*OpnP*) may have resulted in the loss of direct photosensitivity of the pineal gland in owls. Pinopsin is expressed in the pineal gland of birds (Okano et al. 1994) and likely regulates the daily rhythms of melatonin synthesis. Owls have a relatively small and simple pineal with little response to differences in luminance (Taniguchi et al. 1993), which suggests that, similar to mammals, the gland may receive photic input indirectly from the eyes (Falcón et al. 2009). *OpnP* is also inactivated in the penguins *P. adeliae* and *A. forsteri* (Li et al. 2014), but it otherwise appears intact across Aves (Borges et al. 2015). Notably, the loss of pinopsin has also occurred in the historically dim-light-environment-inhabiting Mammalia, Crocodilia, and Serpentes (Walls 1942; Gerkema et al. 2013; Emerling 2017a, 2017b). Crocodilians appear to lack a pineal gland entirely (Roth et al. 1980), whereas mammals have a pineal gland that has moved from a more superficial to a deeper position in the brain (Falcón et al. 2009), presumably resulting in a loss of photosensitivity. Together these data suggest that the loss of direct photosensitivity of the pineal gland is a common theme in amniotes (Tetrapoda: Amniota) that experience minimal exposure to light.

Although we found several putative inactivating mutations in *Opn4m*, these are unlikely to have led to complete loss of function. The shared 4 nt mutation in *T. alba* and *S. o. caurina* suggests that it was inherited from the common ancestor of Strigiformes. If this mutation disrupted the function of *Opn4m* in the common ancestor of Strigiformes, then this gene sequence should have been evolving neutrally in all of the descendant lineages. However, Strigidae and Tytonidae split ~45 million years ago (Prum et al. 2015) yet each ortholog has only accumulated a single additional putative inactivating mutation, both of which are downstream of exon 8. Our dN/dS ratio analyses of crown owl branches yielded an $\omega < 1$ ($\omega = 0.45$), which is consistent with the hypothesis that *Opn4m* remains functional in owls. Furthermore, we were able to assemble *Opn4m* from the retinal mRNA sequences from six additional owls (five strigid and one tytonid), which

indicates that *Opn4m* is still being transcribed in the eyes of those species. We found evidence of multiple *Opn4m* isoforms in the avian retinal transcriptome sequences and the genomic sequences of several other avian taxa possessed putative inactivating mutations. These potentially inactivating mutations were almost all distributed on or after exon 8. Notably, when we used the lowest sensitivity setting of the Geneious aligner to map *Opn4m* BLAST hits from the avian retinal transcriptomes, we primarily obtained assembled sequences that terminated after exon 8. Previous work has found multiple *Opn4m* isoforms in vertebrates (Verra et al. 2011; Hughes et al. 2012). Our results suggest loss of some of these isoforms in owls and other birds. *Opn4m* is involved in entraining circadian rhythms in mammals via the pineal gland, in part, as well as in regulating pupil diameter (Hankins et al. 2008). Given the diminished importance of the pineal gland in owls, alteration of the circadian function of *Opn4m* is a possibility.

CYP2J19 has recently been implicated as the carotenoid ketolase responsible for synthesizing red carotenoids in birds (Lopes et al. 2016; Mundy et al. 2016; Emerling 2017c). Carotenoids, in addition to being involved in pigmentation of avian skin and feathers, are located in oil droplets anterior to the photosensitive outer segments of cone photoreceptors. These oil droplets fine-tune color vision by absorbing shorter wavelengths and reducing spectral overlap between cone visual pigments (Vorobyev 2003). However, these droplets also reduce the number of photons that reach cone photoreceptors and, therefore, may be less beneficial under dim-light conditions. Among owls, *S. aluco*, *Athene noctua* (little owl), and *Asio flammeus* (short-eared owl) are known to possess red cone oil droplets, whereas *Strix uralensis* (Ural owl), *Bubo scandiacus* (snowy owl), and *T. alba* lack them (Erhard 1924; Yew et al. 1977; Bowmaker and Martin 1978; Gondo and Ando 1995). In *S. aluco*, the red oil droplets are limited to <1% of the cone photoreceptor population (Bowmaker and Martin 1978), which is an extremely low proportion compared with other avian species (Bowmaker 1980; Partridge 1989). Additionally, there is recent evidence that *CYP2J19* is inactivated in *T. alba*, is transcribed as a pseudogene in the retinal transcriptome of *Asio otus* (long-eared owl), and is transcribed at low levels in five other owl species as compared with the level observed in diurnal outgroup avian taxa (Emerling 2017c). Among non-owl Aves, the absence of red cone oil droplets has only been reported in two penguin species, *S. humboldti* (Bowmaker and Martin 1985) and *Aptenodytes patagonicus* (Gondo and Ando 1995). Among nonowls, *CYP2J19* is inactivated in the penguins *P. adeliae* and *A. forsteri* as wells as in the kiwi *A. mantelli* (Emerling 2017c), which all forage under dim-light conditions. The *CYP2J19* pseudogene reported here for *S. occidentalis caurina* provides further evidence that owls have repeatedly been losing red carotenoid oil droplets in parallel, potentially to maximize retinal sensitivity in their predominantly nocturnal niche.

Perhaps what is most notable about the loss of light-associated genes in Strigiformes is not the fact that it has occurred, but that it has not ensued to the same extent as in other historically dim-light-adapted vertebrates. Of the nineteen genes we examined, all but one (*CYP2J19*) were likely present in the common ancestor of amniotes (Gerkema et al. 2013; Osborn et al. 2015; Twyman et al. 2016). Excluding *CYP2J19*, mammals lost nine (Mammalia: Marsupialia and Monotremata) to ten of these genes (Mammalia: Placentalia) during a hypothesized nocturnal or mesopic bottleneck (Walls 1942; Heesy and Hall 2010; Davies et al. 2012; Gerkema et al. 2013) and crocodilians lost seven during a similarly hypothesized period of dim-light adaptation (Walls 1942; Emerling 2017a). Among squamates (Reptilia: Squamata), snakes lost seven of these genes during a putative nocturnal and/or fossorial period early in their history, whereas the largely nocturnal geckos lost six (Walls 1942; Emerling 2017b). As for owls, tytonids have lost three of the light-associated genes we examined (*SWS1*, *Rh2*, *OpnP*), whereas strigids have lost only two (*SWS1*, *OpnP*).

Conclusions

We report the first genome of a member of Strigidae, the largest family of owls. We anticipate that this draft whole genome assembly will be useful to those studying the genetics, demography, and conservation of the spotted owl and related taxa. It will be of particular use in genetic identification of hybrid spotted/barred owls (*S. occidentalis* × *varia*) and in ascertaining the frequency of hybridization between these two species in the forests of western North America. The phylogenetic position of owls within Neoaves is at the base of a large clade containing mousebirds (Coliiformes), cuckoo-rollers (Leptosomiformes), trogons (Trongoniformes), hornbills (Bucerotiformes), woodpeckers (Piciformes), and kingfishers (Coraciiformes) (Jarvis et al. 2014; Prum et al. 2015). This placement of owls suggests that our spotted owl genome assembly will be useful in genomic studies that span a substantial component of avian morphologic diversity and life history strategies.

Despite potentially more than 45 million years of dim-light specialization in Strigiformes, owls have retained a diverse array of nonvisual opsin pigments and mechanisms to protect against ultraviolet photo-oxidative damage. Although tytonids have a reduced color vision capacity that is similar to ancestral mammals, crocodilians, and snakes, strigids have retained trichromatic color vision akin to that of humans. Many light-associated gene functions have been maintained in owls, perhaps enabling activities during daylight, a time when most owls are presumed to be generally inactive. It appears that what many consider the quintessential nocturnal birds are not as independent of light as are other nocturnal or crepuscular amniote lineages.

Supplementary Material

Supplementary data are available at *Genome Biology and Evolution* online.

Literature Cited

Altschul SF, et al. 1997. Gapped BLAST and PSI-BLAST: a new generation of protein database search programs. Nucleic Acids Res. 25:3389–3402.

Bao W, Kojima KK, Kohany O. 2015. Repbase Update, a database of repetitive elements in eukaryotic genomes. Mob DNA 6(1): 1–6.

Barrowclough GF, Groth JG, Mertz LA, Gutiérrez RJ. 2005. Genetic structure, introgression, and a narrow hybrid zone between northern and California spotted owls (*Strix occidentalis*). Mol Ecol. 14(4):1109–1120.

Barrowclough GF, Gutierrez RJ, Groth JG. 1999. Phylogeography of spotted owl (*Strix occidentalis*) populations based on mitochondrial DNA sequences: gene flow, genetic structure, and a novel biogeographic pattern. Evolution 53(3): 919–931.

Barrowclough GF, Gutiérrez RJ, Groth JG, Lai JE, Rock DF. 2011. The hybrid zone between northern and california spotted owls in the cascade—sierran suture zone. Condor 113(3):581–589.

Bellingham J, et al. 2006. Evolution of melanopsin photoreceptors: discovery and characterization of a new melanopsin in nonmammalian vertebrates. PLOS Biol. 4(8):e254.

Belterman RHR, Boer LEMD. 1984. A karyological study of 55 species of birds, including karyotypes of 39 species new to cytology. Genetica 65(1):39–82.

Bernt M, et al. 2013. MITOS: Improved de novo metazoan mitochondrial genome annotation. Mol Phylogenet Evol. 69(2):313–319.

Biomatters. 2016a. Geneious. Version 9.1.4. [Accessed 2016 Oct 1]. Available from: http://www.geneious.com.

Biomatters. 2016b. Geneious. Version 9.1.6. [Accessed 2016 Oct 1]. Available from: http://www.geneious.com.

Blackshaw S, Snyder SH. 1999. Encephalopsin: a novel mammalian extra-retinal opsin discretely localized in the brain. J Neurosci. 19: 3681–3690.

Bolger AM, Lohse M, Usadel B. 2014. Trimmomatic: a flexible trimmer for Illumina sequence data. Bioinformatics 30(15):2114–2120.

Borges R, et al. 2015. Gene loss, adaptive evolution and the co-evolution of plumage coloration genes with opsins in birds. BMC Genomics 16:751.

Bowmaker JK. 1980. Colour vision in birds and the role of oil droplets. Trends Neurosci. 3(8):196–199.

Bowmaker JK, Martin GR. 1978. Visual pigments and colour vision in a nocturnal bird, *Strix aluco* (tawny owl). Vision Res. 18(9):1125–1130.

Bowmaker JK, Martin GR. 1985. Visual pigments and oil droplets in the penguin, *Spheniscus humboldti*. J Comp Physiol A 156(1):71–77.

Bradnam K. 2015. Goodbye CEGMA, hello BUSCO! ACGT. [Accessed 2016 Jun 24]. Available from: http://www.acgt.me/blog/2015/5/18/goodbye-cegma-hello-busco.

Bradnam KR, et al. 2013. Assemblathon 2: evaluating de novo methods of genome assembly in three vertebrate species. GigaScience 2(1):10.

Bushnell B. 2014. BBMap. Version 34.00. [Accessed 2016 Oct 1]. Available from: http://sourceforge.net/projects/bbmap/.

Camacho C, et al. 2009. BLAST+: architecture and applications. BMC Bioinformatics 10:421.

Campbell MS, Holt C, Moore B, Yandell M. 2014. Genome annotation and curation using MAKER and MAKER-P. Curr Protoc Bioinformatics Ed. Board Andreas Baxevanis Al 48:4.11.1–4.11.39.

Cantarel BL, et al. 2008. MAKER: an easy-to-use annotation pipeline designed for emerging model organism genomes. Genome Res. 18(1):188–196.

Carleton KL, Spady TC, Cote RH. 2005. Rod and cone opsin families differ in spectral tuning domains but not signal transducing domains as judged by saturated evolutionary trace analysis. J Mol Evol. 61(1):75–89.

CAS:ORN:98821. *CAS Ornithology (ORN). California Academy of Sciences, San Francisco, California, United States of America.* [Accessed 2016 Aug 15]. Available from: http://ipt.calacademy.org: 8080/ipt/resource.do?r=orn.

Castoe TA, et al. 2013. The Burmese python genome reveals the molecular basis for extreme adaptation in snakes. Proc Natl Acad Sci U S A. 110(51):20645–20650.

Clark K, Karsch-Mizrachi I, Lipman DJ, Ostell J, Sayers EW. 2016. GenBank. Nucleic Acids Res. 44(D1):D67–D72.

CMC:ORNI-T:B41533. *CMC ORNI-T. Museum of Natural History & Science, Cincinnati Museum Center, Cincinnati, Ohio, United States of America.*

Consortium TU. 2015. UniProt: a hub for protein information. Nucleic Acids Res. 43(D1):D204–D212.

Courtney SP, et al. 2004. Scientific evaluation of the status of the Northern Spotted Owl. Portland, OR: Sustainable Ecosystems Institute. [Accessed 2013 May 1]. Available from: https://www.fws.gov/oregonfwo/species/Data/NorthernSpottedOwl/BarredOwl/Documents/CourtneyEtAl2004.pdf.

Davies WIL, Collin SP, Hunt DM. 2012. Molecular ecology and adaptation of visual photopigments in craniates. Mol Ecol. 21(13):3121–3158.

Davies WL, et al. 2007. Visual pigments of the platypus: a novel route to mammalian colour vision. Curr Biol. 17:R161–R163.

Davis RJ, Hollen B, Hobson J, Gower JE, Keenum D. 2016. Northwest Forest Plan—the first 20 years (1994-2013): status and trends of northern spotted owl habitats. [Accessed 2016 Oct 7]. Available from: http://www.treesearch.fs.fed.us/pubs/50567.

De Vita R, Cavallo D, Eleuteri P, Dell'Omo G. 1994. Evaluation of interspecific DNA content variations and sex identification in Falconiformes and Strigiformes by flow cytometric analysis. Cytometry 16(4):346–350.

DePristo MA, et al. 2011. A framework for variation discovery and genotyping using next-generation DNA sequencing data. Nat Genet. 43(5):491–498.

Diller LV, et al. 2016. Demographic response of northern spotted owls to barred owl removal. J Wildl Manag. 80(4):691–707.

Doležel J, Bartoš J, Voglmayr H, Greilhuber J. 2003. Letter to the editor. Cytometry A 51(2):127–128.

Dugger KM, et al. 2016. The effects of habitat, climate, and Barred Owls on long-term demography of Northern Spotted Owls. Condor 118(1):57–116.

Edgar RC. 2004. MUSCLE: multiple sequence alignment with high accuracy and high throughput. Nucleic Acids Res. 32(5):1792–1797.

Emerling CA. 2017a. Archelosaurian color vision, parietal eye loss, and the crocodylian nocturnal bottleneck. Mol Biol Evol. 34: 666–676.

Emerling CA. 2017b. Genomic regression of claw keratin, taste receptor and light-associated genes provides insights into biology and evolutionary origins of snakes. Mol Phylogenet Evol. 115:40–49.

Emerling CA. 2017c. Independent pseudogenization of CYP2J19 in penguins, owls and kiwis implicates gene in red carotenoid synthesis. bioRxiv 130468. doi: 10.1101/130468.

Emerling CA, Huynh HT, Nguyen MA, Meredith RW, Springer MS. 2015. Spectral shifts of mammalian ultraviolet-sensitive pigments (short wavelength-sensitive opsin 1) are associated with eye length and photic niche evolution. Proc R Soc B. 282(1819):20151817.

Erhard H. 1924. Messende Untersuchungen über den Farbensinn der Vögel. Zool Jahrb Allg Zool Physiol. 41:489–552.

Falcón J, et al. 2009. Structural and Functional Evolution of the Pineal Melatonin System in Vertebrates. Ann N Y Acad Sci. 1163:101–111.

Finn RD, et al. 2016. The Pfam protein families database: towards a more sustainable future. Nucleic Acids Res. 44(D1):D279–D285.

Fite KV. 1973. Anatomical and behavioral correlates of visual acuity in the great horned owl. Vision Res. 13(2):219.

Forsman ED, et al. 2011. Population Demography of Northern Spotted Owls: Published for the Cooper Ornithological Society. 1st ed. University of California Press: Berkeley and Los Angeles, California. [Accessed 2016 Nov 7]. Available from: http://www.jstor.org/stable/10.1525/j.ctt1pnr7z.

Forsman ED, DeStefano S, Raphael MG, Gutiérrez RJ, eds. 1996. Demography of the Northern Spotted Owl. Lawrence, KS: Allen Press, Inc.

Free Software Foundation. 2012. GNU Awk. Version 4.0.1. [Accessed 2016 Oct 1]. Available from: https://www.gnu.org/software/gawk/.

Fridolfsson A-K, Ellegren H. 1999. A simple and universal method for molecular sexing of non-ratite birds. J Avian Biol. 30(1):116–121.

Funk WC, Forsman ED, Johnson M, Mullins TD, Haig SM. 2010. Evidence for recent population bottlenecks in northern spotted owls (*Strix occidentalis caurina*). Conserv Genet. 11(3):1013–1021.

Funk WC, Forsman ED, Mullins TD, Haig SM. 2008. Introgression and dispersal among spotted owl (*Strix occidentalis*) subspecies. Evol Appl. 1(1):161–171.

GBE

Funk WC, Mullins TD, Forsman ED, Haig SM. 2007. Microsatellite loci for distinguishing spotted owls (*Strix occidentalis*), barred owls (*Strix varia*), and their hybrids. Mol Ecol Notes 7(2):284–286.

Gerkema MP, Davies WIL, Foster RG, Menaker M, Hut RA. 2013. The nocturnal bottleneck and the evolution of activity patterns in mammals. Proc R Soc B Biol Sci. 280(1765):20130508.

Gnerre S, et al. 2011. High-quality draft assemblies of mammalian genomes from massively parallel sequence data. Proc Natl Acad Sci U S A. 108(4):1513–1518.

Gondo M, Ando H. 1995. Comparative and histophysiological study of oil droplets in the avian retina. Kobe J Med Sci. 41(4):127–139.

Gremme G, Steinbiss S, Kurtz S. 2013. GenomeTools: a comprehensive software library for efficient processing of structured genome annotations. IEEE/ACM Trans Comput Biol Bioinform. 10:645–656.

Guan X, Xu J, Smith EJ. 2016. The complete mitochondrial genome sequence of the budgerigar, *Melopsittacus undulatus*. Mitochondrial DNA A Mapp Seq Anal. 27(1):401–402.

Haig SM, Mullins TD, Forsman ED, Trail PW, Wennerberg L. 2004. Genetic identification of spotted owls, barred owls, and their hybrids: legal implications of hybrid identity. Conserv Biol. 18(5):1347–1357.

Haig SM, Wagner RS, Forsman ED, Mullins TD. 2001. Geographic variation and genetic structure in Spotted Owls. Conserv Genet. 2(1):25–40.

Halford S, et al. 2001. Characterization of a novel human opsin gene with wide tissue expression and identification of embedded and flanking genes on chromosome 1q43. Genomics 72(2):203–208.

Hamer TE, Forsman ED, Fuchs AD, Walters ML. 1994. Hybridization between barred and spotted owls. Auk 111(2):487–492.

Hammar B. 1970 2009. The karyotypes of thirty-one birds. Hereditas 65(1):29–58.

Hankins MW, Peirson SN, Foster RG. 2008. Melanopsin: an exciting photopigment. Trends Neurosci. 31(1):27–36.

Hanna ZR, et al. 2017. Supplemental dataset for Northern Spotted Owl (*Strix occidentalis caurina*) genome assembly version 1.0. Zenodo doi: 10.5281/zenodo.822859.

Harrison GL, et al. 2004. Four new avian mitochondrial genomes help get to basic evolutionary questions in the late cretaceous. Mol Biol Evol. 21(6):974–983.

Heesy CP, Hall MI. 2010. The nocturnal bottleneck and the evolution of mammalian vision. Brain Behav Evol. 75(3):195–203.

Henderson JB, Hanna ZR. 2016a. dupchk. Version 1.0.0. Zenodo. DOI: 10.5281/zenodo.163722.

Henderson JB, Hanna ZR. 2016b. GItaxidlsVert. Version 1.0.0. Zenodo. DOI: 10.5281/zenodo.163737.

Henderson JB, Hanna ZR. 2016c. ScaffSplitN50s. Version 1.0.0. Zenodo. DOI: 10.5281/zenodo.163683.

Henderson JB, Hanna ZR. 2016d. scafN50. Version 1.0.0. Zenodo. DOI: 10.5281/zenodo.163739.

Henderson JB, Hanna ZR. 2016e. scafSeqContigInfo. Version 1.0.0. Zenodo. DOI: 10.5281/zenodo.163748.

Hengjiu T, et al. 2016. Complete mitochondrial genome of Eagle Owl (*Bubo bubo*, Strigiformes; Strigidae) from China. Mitochondrial DNA A 27(2):1455–1456.

Hsu Y-C, Li S-H, Lin Y-S, Severinghaus LL. 2006. Microsatellite loci from lanyu scops owl (*Otus elegans botelensis*) and their cross-species application in four species of strigidae. Conserv Genet. 7(1):161–165.

Hsu Y-C, Severinghaus LL, Lin Y-S, Li S-H. 2003. Isolation and characterization of microsatellite DNA markers from the Lanyu scops owl (*Otus elegans botelensis*). Mol Ecol Notes 3(4):595–597.

Hudson RR, Slatkin M, Maddison WP. 1992. Estimation of levels of gene flow from DNA sequence data. Genetics 132(2):583–589.

Hughes S, et al. 2012. Differential expression of melanopsin isoforms Opn4L and Opn4S during postnatal development of the mouse retina. PLoS One 7(4):e34531.

Hunter JD. 2007. Matplotlib: A 2D graphics environment. Comput Sci Eng. 9(3):90–95.

Ihnat DM, MacKenzie D, Meyering J. 2013. cut (GNU coreutils). Version 8.21. [Accessed 2016 Oct 1]. Available from http://www.gnu.org/software/coreutils/coreutils.html.

Isaksson M, Tegelström H. 2002. Characterization of polymorphic microsatellite markers in a captive population of the eagle owl (Bubo bubo) used for supportive breeding. Mol Ecol Notes 2(2):91–93.

Jacobs GH. 2013. Losses of functional opsin genes, short-wavelength cone photopigments, and color vision—A significant trend in the evolution of mammalian vision. Vis Neurosci. 30(1–2): 39–53.

Jarvis ED, et al. 2014. Whole-genome analyses resolve early branches in the tree of life of modern birds. Science 346(6215):1320–1331.

Jennings S, Cormier RL, Gardali T, Press D, Merkle WW. 2011. Status and distribution of the barred owl in Marin County, California. West Birds 42:103–110.

Jones P, et al. 2014. InterProScan 5: genome-scale protein function classification. Bioinformatics 30(9):1236–1240.

Jurka J. 2000. Repbase Update: a database and an electronic journal of repetitive elements. Trends Genet. 16(9):418–420.

Jurka J, et al. 2005. Repbase Update, a database of eukaryotic repetitive elements. Cytogenet. Genome Res. 110(1–4):462–467.

Jurka J. 1998. Repeats in genomic DNA: mining and meaning. Curr Opin Struct Biol. 8(3):333–337.

Kato T, et al. 1994. Cloning of a marsupial DNA photolyase gene and the lack of related nucleotide sequences in placental mammals. Nucleic Acids Res. 22(20):4119–4124.

Kearse M, et al. 2012. Geneious Basic: an integrated and extendable desktop software platform for the organization and analysis of sequence data. Bioinformatics 28(12):1647–1649.

Keller O, Kollmar M, Stanke M, Waack S. 2011. A novel hybrid gene prediction method employing protein multiple sequence alignments. Bioinformatics 27(6):757–763.

Kelly EG, Forsman ED. 2004. recent records of hybridization between barred owls (*Strix varia*) and northern spotted owls (*S. occidentalis caurina*). Auk 121(3):806–810.

Koopman ME, Schable NA, Glenn TC. 2004. Development and optimization of microsatellite DNA primers for boreal owls (*Aegolius funereus*). Mol Ecol Notes 4(3):376–378.

Korf I. 2004. Gene finding in novel genomes. BMC Bioinformatics 5:1–9.

Le Duc D, et al. 2015. Kiwi genome provides insights into evolution of a nocturnal lifestyle. Genome Biol. 16(1):1–15.

Leinonen R, Sugawara H, Shumway M. 2011. The sequence read archive. Nucleic Acids Res. 39(Database issue):D19–D21.

Li C, et al. 2014. Two Antarctic penguin genomes reveal insights into their evolutionary history and molecular changes related to the Antarctic environment. GigaScience 3(1):1–15.

Li H. 2013a. Aligning sequence reads, clone sequences and assembly contigs with BWA-MEM. ArXiv13033997 Q-Bio. [Accessed 2016 Feb 16]. Available from: http://arxiv.org/abs/1303.3997.

Li H. 2013b. bioawk. Version 1.0. [Accessed 2016 Oct 1]. Available from: https://github.com/lh3/bioawk.

Li H. 2015. PSMC. [Accessed 2016 Oct 1]. Version 0.6.5-r67. Available from: https://github.com/lh3/psmc.

Li H, Durbin R. 2011. Inference of human population history from individual whole-genome sequences. Nature 475(7357):493–496.

Liu G, Zhou L, Gu C. 2014. The complete mitochondrial genome of Brown wood owl *Strix leptogrammica* (Strigiformes: Strigidae). Mitochondrial DNA 25(5):370–371.

Livezey KB. 2009. Range expansion of barred owls, part i: chronology and distribution. Am Midl Nat. 161(1):49–56.

Livezey KB. 2009. Range Expansion of Barred Owls, Part II: Facilitating Ecological Changes. Am Midl Nat. 161(2):323–349.

Lopes RJ, et al. 2016. Genetic basis for red coloration in birds. Curr Biol. 26(11):1427–1434.

Luo R, et al. 2012. SOAPdenovo2: an empirically improved memory-efficient short-read de novo assembler. GigaScience 1(1):18.

Mahmood MT, McLenachan PA, Gibb GC, Penny D. 2014. Phylogenetic position of avian nocturnal and diurnal raptors. Genome Biol Evol. 6(2):326–332.

Mazur KM, James PC. 2000. Barred Owl (*Strix varia*). In: Poole A, editor. The birds of North America online. Ithaca: Cornell Lab of Ornithology. [Accessed 2016 Oct 1]. Retrieved from the Birds of North America Online: https://birdsna.org/Species-Account/bna/species/brdowl. doi: 10.2173/bna.508.

McKenna A, et al. 2010. The Genome Analysis Toolkit: a MapReduce framework for analyzing next-generation DNA sequencing data. Genome Res. 20(9):1297–1303.

Mindell DP, et al. 1999. Interordinal relationships of birds and other reptiles based on whole mitochondrial genomes. Syst Biol. 48(1):138–152.

Mindell DP, et al. 1997. Phylogenetic Relationships among and within Select Avian Orders Based on Mitochondrial DNA. In: Avian Molecular Evolution and Systematics. San Diego, California: Academic Press, p. 213–247.

Mindell DP, Sorenson MD, Dimcheff DE. 1998. Multiple independent origins of mitochondrial gene order in birds. Proc Natl Acad Sci U S A. 95(18):10693–10697.

Mundy NI, et al. 2016. Red carotenoid coloration in the zebra finch is controlled by a cytochrome P450 gene cluster. Curr Biol. 26(11):1435–1440.

Nakamura D, Tiersch TR, Douglass M, Chandler RW. 1990. Rapid identification of sex in birds by flow cytometry. Cytogenet Cell Genet. 53(4):201–205.

NCBI Resource Coordinators 2016. Database resources of the National Center for Biotechnology Information. Nucleic Acids Res. 44(D1):D7–D19.

O'Connell J, et al. 2015. NxTrim: optimized trimming of Illumina mate pair reads. Bioinformatics 31(12):2035–2037.

O'Connell J. 2014. NxTrim. Version 0.2.3-alpha. [Accessed 2016 Oct 1]. Available from: https://github.com/sequencing/NxTrim.

Okano T, Yoshizawa T, Fukada Y. 1994. Pinopsin is a chicken pineal photoreceptive molecule. Nature 372(6501):94–97.

Osborn AR, et al. 2015. De novo synthesis of a sunscreen compound in vertebrates. eLife 4:e05919.

Parra G, Bradnam K, Korf I. 2007. CEGMA: a pipeline to accurately annotate core genes in eukaryotic genomes. Bioinformatics 23(9):1061–1067.

Partridge JC. 1989. The visual ecology of avian cone oil droplets. J Comp Physiol A 165(3):415–426.

Proudfoot G, Honeycutt R, Douglas Slack R. 2005. Development and characterization of microsatellite DNA primers for ferruginous pygmy-owls (*Glaucidium brasilianum*). Mol Ecol Notes 5(1):90–92.

Prum RO, et al. 2015. A comprehensive phylogeny of birds (Aves) using targeted next-generation DNA sequencing. Nature 526(7574):569–573.

Rebholz WER, et al. 1993. The chromosomal phylogeny of owls (Strigiformes) and new karyotypes of seven species. Cytologia (Tokyo) 58(4):403–416.

Renzoni A, Vegni-Talluri M. 1966. The karyograms of some Falconiformes and Strigiformes. Chromosoma 20(2):133–150.

Roth JJ, Gern WA, Roth EC, Ralph CL, Jacobson E. 1980. Nonpineal melatonin in the alligator (*Alligator mississippiensis*). Science 210(4469):548–550.

Shen D, et al. 1994. A human opsin-related gene that encodes a retinaldehyde-binding protein. Biochemistry (Mosc.) 33(44):13117–13125.

Simão FA, Waterhouse RM, Ioannidis P, Kriventseva EV, Zdobnov EM. 2015a. BUSCO: assessing genome assembly and annotation completeness with single-copy orthologs. Bioinformatics 31(19):3210–3212.

Simão FA, Waterhouse RM, Ioannidis P, Kriventseva EV, Zdobnov EM. 2015b. BUSCO. Version 1.1b1. [Accessed 2016 Oct 1]. Available from: http://busco.ezlab.org.

Simões BF, et al. 2015. Visual system evolution and the nature of the ancestral snake. J Evol Biol. 28: 1309–1320.

Simpson JT. 2014. Exploring genome characteristics and sequence quality without a reference. Bioinformatics 30(9):1228–1235.

Smit A, Hubley R, Green P. 2013. RepeatMasker Open-4.0. [Accessed 2016 Oct 1]. Available from: http://www.repeatmasker.org.

Smit AFA, Hubley R. 2015. RepeatModeler Open-1.0. [Accessed 2016 Oct 1]. Available from: http://www.repeatmasker.org.

Soni BG, Foster RG. 1997. A novel and ancient vertebrate opsin. FEBS Lett. 406(3):279–283.

Stanke M. 2015. AUGUSTUS. Version 3.2.1. [Accessed 2016 Oct 1]. Available from: http://bioinf.uni-greifswald.de/augustus.

Sun H, Gilbert DJ, Copeland NG, Jenkins NA, Nathans J. 1997. Peropsin, a novel visual pigment-like protein located in the apical microvilli of the retinal pigment epithelium. Proc Natl Acad Sci USA. 94: 9893–9898.

Taniguchi M, et al. 1993. Melatonin release from pineal cells of diurnal and nocturnal birds. Brain Res. 620(2):297–300.

Tarttelin EE, et al. 2003. Expression of opsin genes early in ocular development of humans and mice. Exp Eye Res. 76(3):393–396.

Taylor AL, Forsman ED. 1976. Recent range extensions of the Barred Owl in western North America, including the first records for Oregon. Condor 78(4):560–561.

Thode AB, Maltbie M, Hansen LA, Green LD, Longmire JL. 2002. Microsatellite markers for the Mexican spotted owl (*Strix occidentalis lucida*). Mol Ecol Notes 2(4):446–448.

Thomas JW, et al. 1990. A conservation strategy for the northern spotted owl. A report by the Interagency Scientific Committee to address the conservation of the northern spotted owl. USDA Forest Service; USDI Bureau of Land Management, Fish and Wildlife Service, National Park Service: Portland, Oregon.

Toews DPL, et al. 2016. Plumage genes and little else distinguish the genomes of hybridizing warblers. Curr Biol. 26(17):2313–2318.

Tomonari S, Migita K, Takagi A, Noji S, Ohuchi H. 2008. Expression patterns of the opsin 5–related genes in the developing chicken retina. Dev Dyn. 237(7):1910–1922.

Twyman H, Valenzuela N, Literman R, Andersson S, Mundy NI. 2016. Seeing red to being red: conserved genetic mechanism for red cone oil droplets and co-option for red coloration in birds and turtles. Proc R Soc B 283(1836):20161208.

Van der Auwera GA, et al. 2013. From FastQ data to high confidence variant calls: the Genome Analysis Toolkit best practices pipeline. Curr Protoc Bioinforma 11:11.10.1–11.10.33.

Verra DM, Contín MA, Hicks D, Guido ME. 2011. Early onset and differential temporospatial expression of melanopsin isoforms in the developing chicken retina. Invest Ophthalmol Vis Sci. 52: 5111–5120.

Vinogradov AE. 2005. Genome size and chromatin condensation in vertebrates. Chromosoma 113(7):362–369.

Vonk FJ, et al. 2013. The king cobra genome reveals dynamic gene evolution and adaptation in the snake venom system. Proc Natl Acad Sci U S A. 110(51):20651–20656.

Vorobyev M. 2003. Coloured oil droplets enhance colour discrimination. Proc R Soc Lond B Biol Sci. 270(1521):1255–1261.

Walls GL. 1942. The vertebrate eye and its adaptive radiation. Cranbrook Institute of Science: Bloomfield Hills, Michigan. doi: 10.5962/bhl.title.7369.

Warren W, et al. 2014. Genomic data of the Bald Eagle (*Haliaeetus leucocephalus*). GigaScience Database. doi: 10.5524/101040.

Warren W, Bussche RAVD, Minx P. 2014. Direct Submission. Aquila chrysaetos canadensis isolate GSEH35GE, whole genome shotgun sequencing project submitted (09-OCT-2014) to NCBI accession JRUM00000000.1. The Genome Institute, Washington University School of Medicine, St Louis, Missouri, U.S.A.

Warren WC, et al. 2017. A new chicken genome assembly provides insight into avian genome structure. G3: Genes|Genomes|Genetics 7(1): 109–117.

Warren WC, et al. 2010. The genome of a songbird. Nature 464(7289):757–762.

Wheeler TJ, et al. 2013. Dfam: a database of repetitive DNA based on profile hidden Markov models. Nucleic Acids Res. 41(D1):D70–D82.

Wicker T, et al. 2005. The repetitive landscape of the chicken genome. Genome Res. 15:126–136.

Wiens JD, Anthony RG, Forsman ED. 2014. Competitive interactions and resource partitioning between northern spotted owls and barred owls in western Oregon. Wildl Monogr. 185(1):1–50.

Wu Y, et al. 2016. Retinal transcriptome sequencing sheds light on the adaptation to nocturnal and diurnal lifestyles in raptors. Sci Rep. 6:33578.

Yamada K, Nishida-Umehara C, Matsuda Y. 2004. A new family of satellite DNA sequences as a major component of centromeric heterochromatin in owls (Strigiformes). Chromosoma 112(6):277–287.

Yang Z. 2007. PAML 4: phylogenetic analysis by maximum likelihood. Mol Biol Evol. 24(8):1586–1591.

Yates A, et al. 2016. 2016. Ensembl 2016. Nucleic Acids Res. 44(D1):D710–D716.

Yew DT, Woo HH, Meyer DB. 1977. Further studies on the morphology of the owl's retina. Cells Tissues Organs 99(2):166–168.

Zhang G, Li B, Li C, et al. 2014. Comparative genomic data of the Avian Phylogenomics Project. GigaScience 3(1):1–8.

Zhang G, Li C, et al. 2014. Comparative genomics reveals insights into avian genome evolution and adaptation. Science 346(6215): 1311–1320.

Zhang G, Li B, Gilbert M, et al. 2014a. Genomic data of the Barn owl (*Tyto alba*). GigaScience Database. doi: 10.5524/101039.

Zhang G, Li B, Gilbert M, et al. 2014b. Genomic data of the Downy Woodpecker (*Picoides pubescens*). GigaScience Database. doi: 10.5524/101012.

Zhang G, Li B, Gilbert M, et al. 2014c. Genomic data of the Chimney Swift (*Chaetura pelagica*). GigaScience Database. doi: 10.5524/101005.

Zhang Y, et al. 2016. Complete sequence and gene organization of the mitochondrial genome of *Asio flammeus* (Strigiformes, strigidae). Mitochondrial DNA A 27:2665–2667.

Zhang Z, Schwartz S, Wagner L, Miller W. 2000. A greedy algorithm for aligning DNA sequences. J Comput Biol. 7(1–2):203–214.

Associate editor: Dorothée Huchon